Journal of Controlled Release 293 (2019) 113–125

Contents lists available at ScienceDirect

Journal of Controlled Release

journal homepage: www.elsevier.com/locate/jconrel

Folate-dactolisib conjugates for targeting tubular cells in polycystic kidneys

Haili Shi[a], Wouter N. Leonhard[b], Niels J. Sijbrandi[c], Mies J. van Steenbergen[a], Marcel H.A.M. Fens[a], Joep B. van de Dikkenberg[a], Javier Sastre Toraño[d], Dorien J.M. Peters[b], Wim E. Hennink[a], Robbert Jan Kok[a,*]

[a] Department of Pharmaceutics, Utrecht Institute for Pharmaceutical Sciences, Utrecht University, Utrecht, The Netherlands
[b] Department of Human Genetics, Leiden University Medical Center, Leiden, The Netherlands
[c] LinXis B.V., Amsterdam, The Netherlands
[d] Department of Chemical Biology and Drug Discovery, Utrecht Institute for Pharmaceutical Sciences, Utrecht University, Utrecht, The Netherlands

ARTICLE INFO

Keywords:
Drug targeting
Coordination chemistry
Receptor-mediated uptake
Signal transduction

ABSTRACT

The aim of the present study was to develop folic acid (FA) conjugates which can deliver the kinase inhibitor dactolisib to the kidneys via folate receptor-mediated uptake in tubular epithelial cells. Dactolisib is a dual inhibitor of phosphatidylinositol 3-kinase (PI3K) and mammalian target of rapamycin (mTOR) and is considered an attractive agent for treatment of polycystic kidney disease. The ethylenediamine platinum(II) linker, herein called Lx, was employed to couple dactolisib via coordination chemistry to thiol-containing FA-spacer adducts to yield FA-Lx-dactolisib conjugates. The dye lissamine was coupled via similar linker chemistry to folate to yield fluorescent FA-Lx-lissamine conjugates. Three different spacers (PEG_5-Cys, PEG_{27}-Cys or an Asp-Arg-Asp-Asp-Cys peptide spacer) were used to compare the influence of hydrophilicity and charged groups in the spacer on interaction with target cells and in vivo organ distribution of the final conjugates. The purity and identity of the final products were confirmed by UPLC and LC-MS analysis, respectively. FA-Lx-dactolisib conjugates were stable in serum and culture medium, while dactolisib was released from the conjugates in the presence of glutathione. All three type of conjugates were internalized efficiently by HK-2 cells and uptake could be blocked by an excess of folic acid in the medium, demonstrating FR mediated uptake. FA-Lx-dactolisib conjugates showed nanomolar inhibition of the PI3K pathway (Akt phosphorylation) and mTOR pathway (S6 phosphorylation) in cultured kidney epithelial cells (HK-2 cells). After intraperitoneal administration, all three types conjugates accumulated extensively in kidneys of iKsp-*Pkd1*^{del} mice with polycystic kidney disease. In conclusion, folate conjugates were successfully prepared by platinum(II) coordination chemistry and accumulated in a target-specific manner in kidney cells and polycystic kidneys. The folate conjugate of dactolisib thus may have potential for targeted therapy of polycystic kidney disease.

1. Introduction

The folate receptor (FR), also known as the high affinity membrane folate binding protein, is a glycosylphosphatidylinositol (GPI)-linked membrane glycoprotein with a molecular weight of 38–40 kDa and is significantly upregulated in many cancer cells [1]. A range of folate-drug conjugates has been developed for targeted delivery of anticancer drugs to various types of tumors [2–6]. Importantly, high expression of the folate receptor has also been observed in the kidney, particularly on the apical brush-border membrane of kidney proximal tubule cells [7–9]. Thus, although designated for targeting cancer cells, low-molecular-weight folate conjugates such as [^{99m}Tc]DTPA-folate accumulated substantially in the kidneys when intravenously administered [10]. Studies with folate-drug conjugates in non-cancerous disease showed successful targeting and therapeutic responses in adjuvant arthritis [11–13] and in kidney disease models [14,15].

Autosomal dominant polycystic kidney disease (ADPKD) is one of the most common genetic kidney diseases, which often leads to end-stage renal failure [16–19]. The incidence of this disease is estimated to be 1:2500 in the European Union (EU) [20]. ADPKD is characterized by the progressive development of fluid-filled kidney cysts which replace the normal renal parenchyma ultimately resulting in loss of kidney function [21]. ADPKD is caused by heterozygous mutations in the *Pkd1* (85% of the patients) and *Pkd2* gene (15% of the patients) [22,23]. Currently, there are no effective treatments for ADPKD patients and most of them rely on kidney transplantation therapy [24]. New

* Corresponding author.
E-mail address: r.j.kok@uu.nl (R.J. Kok).

https://doi.org/10.1016/j.jconrel.2018.11.019
Received 4 June 2018; Received in revised form 14 November 2018; Accepted 20 November 2018
Available online 23 November 2018

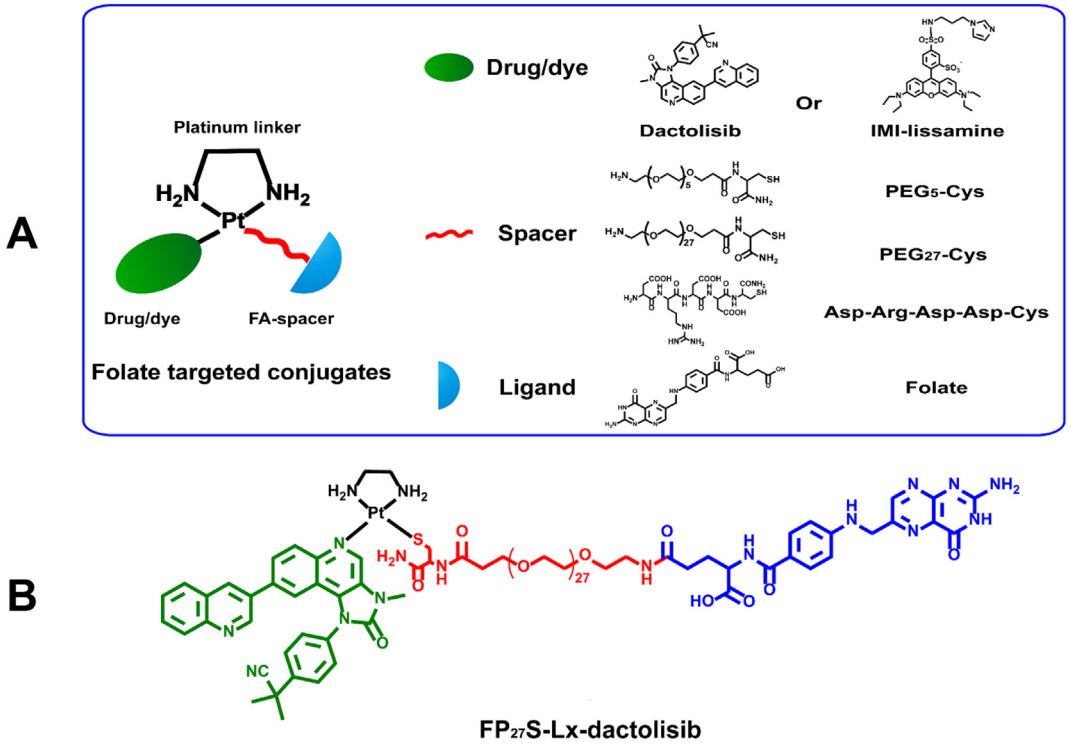

Fig. 1. (A) Design of folate targeted drug conjugates FA-Lx-dactolisib and FA-Lx-lissamine using platinum linker. It consists of four parts: the drug dactolisib and fluorescent agent lissamine, the metal-organic platinum linker Lx, the hydrophilic spacers PEG_5-Cys, PEG_{27}-Cys and Asp-Arg-Asp-Asp-Cys peptide, and the targeting ligand folate. (B) Chemical structure of FP_{27}S-Lx-dactolisib, a representative folate targeted conjugate.

treatments for ADPKD under development are mainly focused on targeting the dysregulated signaling pathways in the disease. Several studies have revealed that both the mammalian target of rapamycin (mTOR) and phosphatidylinositol 3-kinase (PI3K) pathways are activated by PC-1 expression which is encoded by the *Pkd1* gene in ADPKD [25,26].

Dactolisib, also known as NVP-BEZ235 or BEZ235 (chemical structure shown in Fig. 1), is a dual inhibitor of PI3K/mTOR signaling pathways which both play an important role in cell proliferation and cell cycle [27–29]. Dactolisib has entered clinical trials in patients with renal cell carcinoma but has been discontinued due to a high incidence of gastrointestinal side effects [30]. As mentioned above, PI3K/mTOR signaling pathways are also involved in the pathogenesis of ADPKD. In a recent study using 3D-cultured kidney cysts, Booij et al. have shown potent inhibitory effects of dactolisib on cystic growth [31]. Moreover, dactolisib was reported effective in a mouse model of ADPKD [32]. In the present study, dactolisib was selected for the design of folate containing prodrug conjugates which can be used for targeted delivery to polycystic kidneys.

Most drug conjugates contain an ester, amide, disulfide or hydrazone bond that facilitates covalent and bioreversible conjugation of the drug to the targeting ligand. [33] Since dactolisib lacks functional groups (such as −OH, $-NH_2$, −COOH and −SH) that can be exploited for the above conjugation reactions, we explored an alternative coupling strategy. Dactolisib contains quinoline groups, which can form coordinative N−Pt bonds with the metal-organic linker dichloro(ethylenediamine)platinum(II), herein called Lx [34–37]. In the next step, Lx-dactolisib complex was coupled to hydrophilic folate-spacer adducts comprising a thiol group which also forms coordination linkages with the platinum(II) coordinative center, yielding the final FA-Lx-dactolisib conjugates. The Lx-dactolisib complex is positively charged which increases the water solubility of the dactolisib conjugates. Since dactolisib has a very low aqueous solubility (log $P = 5.2$ [38]), it can be anticipated however that the charge of the linker will not provide enough water solubility. Therefore, three different hydrophilic spacers PEG_5-Cys, PEG_{27}-Cys and Asp-Arg-Asp-Asp-Cys peptide were developed to increase the aqueous solubility of the final conjugates and to avoid possible aggregation and nonspecific uptake of the conjugates by cells as shown for other drug-targeting ligand conjugates [39]. Differences in hydrophilicity and charged groups within the spacers may furthermore influence the interaction with FR -thus affecting uptake in target cells- or undesired interactions that determine the organ distribution of small drug-carrier conjugates. To study these processes further, fluorescent FA-Lx-lissamine conjugates were synthesized which had similar hydrophilic spacers and a platinum(II)-coordinative linker center. The overall synthesis strategy of preparation of folate conjugates is shown in Fig. 1.

The conjugates were prepared by solid phase synthesis and purified by preparative HPLC, while identity of their structures was confirmed by LC-MS analysis. The stability and drug release properties of the conjugates were investigated under normal conditions and in the presence of compounds that can release dactolisib from the coordinative linker such as gluthathione (GSH) and dithiothreitol (DTT). The inhibition of PI3K/mTOR signaling pathways was evaluated in cultured kidney epithelial cells by western blotting of the signaling pathways targeted by dactolisib. The cellular uptake of FA-Lx-lissamine fluorescent conjugates in kidney epithelial cells was studied by confocal fluorescence microscopy. Finally, we confirmed the accumulation of FA-Lx-lissamine conjugates in polycystic kidney after i.p. administration. Our results demonstrate that this newly developed class of folate conjugates can specifically target the polycystic kidney. The linking approach with platinum(II) coordinative linkers offers new possibilities for conjugating potent inhibitors to folate and other ligands that can facilitate for targeted uptake in tubular cells in the polycystic kidney.

2. Materials and methods

2.1. Materials

Dactolisib was purchased from LC Laboratories (Woburn, USA). TentaGel® S RAM resin was purchased from Rapp Polymere (Tuebingen, Germany). N^{10}-(trifluoroacetyl)pteroic acid was purchased from Carbosynth (Berkshire, UK). Fmoc-L-Glu-OtBu, Fmoc-NH-PEG_5-COOH and Fmoc-NH-PEG_{27}-COOH were purchased from Iris Biotech GmbH (Marktredwitz, Germany). Syringe peptide synthesis vessels were purchased from Screening Devices BV (Amersfoort, The Netherlands). Dichloro(ethylenediamine)platinum(II) [$PtCl_2$(en)], lissamine™ rhodamine B, Fmoc-Cys(Trt)-OH, Fmoc-Asp(OtBu)-OH, Fmoc-Arg(Pbf)-OH, folic acid, silver nitrate, tricine, thiourea, sodium nitrate, *N*-hydroxysuccinimide (NHS), *N,N′*-dicyclohexylcarbodimide (DCC), ethylenediamine (EDA), potassium thiocyanate (KSCN), 4-dimethylaminopyridine (DMAP), 1-hydroxy-benzotriazole (HOBt), triisopropylsilane (TIPS), 1,2-ethanedithiol (EDT), (benzotriazol-1-yloxy)tris-(dimethylamino)phosphonium hexafluorophosphate (BOP), *N,N′*-diisopropylethylamine (DIPEA), piperidine, hydrazine, acetic anhydride, formic acid, L-glutathione (GSH), DL-dithiothreitol (DTT), trifluoroacetic acid (TFA), tris base, sodium chloride, Tween 20, hematoxylin and eosin Y were purchased from Sigma-Aldrich (Zwijndrecht, The Netherlands). Dimethyl sulfoxide (DMSO), diethyl ether, acetonitrile, peptide grade *N,N*-dimethylformamide (DMF) and dichloromethane (DCM) were purchased from Biosolve BV (Valkenswaard, The Netherlands). All cell culture materials were ordered from Gibco (Grand Island, NY, USA). NuPAGE 4–12% Bis-Tris protein gels and NuPAGE MOPS SDS running buffer were purchased from Invitrogen (Breda, The Netherlands). Phospho-S6 ribosomal protein (Ser240/244) rabbit antibody, phospho-Akt (Ser473) rabbit mAb, β-Actin rabbit mAb and horseradish peroxidase (HRP)-conjugated goat anti-rabbit secondary antibody were purchased from Cell Signaling Technology (Leiden, The Netherlands). RIPA buffer, protease and phosphatase inhibitors, rabbit anti-folate primary antibody and donkey anti-rabbit IgG (H + L) Alexa Fluor 488 secondary antibody were purchased from Thermofisher Scientific (Karlsruhe, Germany). FluorSave™ Reagent was ordered from Millipore (Amsterdam, the Netherlands).

2.2. UPLC, NMR, LC-MS and Preparative HPLC

2.2.1. Ultraperformance liquid chromatography (UPLC)

The purity of the synthesized conjugates was evaluated by UPLC using a Waters ACQUITY system (Waters Associates Inc., Milford, MA, USA) equipped with an ACQUITY UPLC CSH C18 column (2.1 × 50 mm). The mobile phase consisted of two solvents (Eluent A: water/acetonitrile = 95/5 (*v*/v) with 0.1% formic acid; eluent B: acetonitrile with 0.1% formic acid). All the compounds were eluted using a linear gradient: 0% B to 60% B in 2.5 min at a flow rate of 0.5 ml/min. The injection volume was 5 µl. The detection wavelength for FA-PEG_5-SH (FP_5S), FA-PEG_{27}-SH ($FP_{27}S$), FA-Asp-Arg-Asp-Asp-SH (FAS) and Fmoc-PEG_5-SH ($FmocP_5S$) was 290 nm. The detection wavelength for dactolisib, Lx-dactolisib and FA-Lx-dactolisib conjugates (synthesized as described in Section 2.5) was 340 nm. The detection wavelength for lissamine, IMI-lissamine, FA-Lx-lissamine and $FmocP_5S$-Lx-lissamine conjugates (Section 2.5) was 560 nm [40–42]. The chromatograms were analyzed using Empower Software.

2.2.2. Nuclear magnetic resonance (NMR)

^{1}H NMR spectra of the synthesized Lx-dactolisib dissolved in DMSO-d_6 were recorded at 25 °C with an Agilent 400 MHz spectrometer (Santa Clara, CA, USA). The central line of DMSO at 2.5 ppm was used as reference line.

2.2.3. Liquid chromatography-mass spectrometry (LC-MS)

LC-MS analyses were performed on a Thermo Finnigan UPLC system (Thermo Finnigan, San Jose, CA, USA) coupled to a Bruker Q-TOF mass spectrometer (Bremen, Germany) equipped with an electrospray ionization (ESI) source. An ACQUITY UPLC CSH C18 column (2.1 × 50 mm) was used for separation. A binary solvent system of water/acetonitrile (LC-MS Grade) 95:5 (*v*/v) with 0.1% formic acid (solvent A) and acetonitrile (LC-MS Grade) with 0.1% formic acid (solvent B) were used as the mobile phase. The eluting gradient, flow rate and injection volume were the same as those used for UPLC analysis. Mass analysis was conducted in positive ionization mode under the following settings: nebulizer pressure, 70.0 bar; drying gas flow rate, 12 l/min; drying gas temperature, 35 °C; ESI voltage, 4.5 kV; scan range, 50 to 3000 *m/z*. Data analysis was conducted on Bruker Daltonics Data Analysis software.

2.2.4. Preparative-high performance liquid chromatography (Prep-HPLC)

Purification of the synthesized conjugates was performed on a Waters preparative HPLC system using an XBridge BEH C18 OBD Prep column (19 × 150 mm). Eluent A: water/acetonitrile = 95/5 (*v*/v) with 0.1% formic acid; eluent B: acetonitrile with 0.1% formic acid. Method: 20% B to 60% B in 30 min at a flow rate of 20 ml/min for all the compounds. The injection volume was 4 ml with a concentration of 20 mg/ml.

2.3. Solid phase synthesis of FA-spacer adducts

2.3.1. Synthesis of FA-PEG_5-SH (FP_5S)

The solid phase synthesis of FA-PEG_5-SH includes six steps (Fig. 2). In detail, Fmoc-2, 4-dimethoxy-4′-(carboxymethyloxy)-benzhydrylamine aminomethyl resin (TentaGel® S RAM) (0.535 g, 0.118 mmol) was transferred into a peptide synthesis vessel. Next, 5 ml dry DMF was added to swell the resin. After 30 mins, the Fmoc groups which protect the -NH_2 on the resin were removed by 20% piperidine in DMF (2 × 9 ml) [43]. Subsequently, Fmoc-Cys(Trt)-OH (206 mg, 0.354 mmol), BOP (1 equiv) and DIPEA (1.5 equiv) in DMF were introduced into the reaction vessel. After flushing with N_2 at room temperature for 1 h, the peptide-resin was subsequently washed with DMF (3 × 5 ml) and DCM (3 × 5 ml). Next, 20% piperidine in DMF (2 × 9 ml) was used to remove the Fmoc group. Fmoc-NH-PEG_5-COOH (203 mg, 0.354 mmol), Fmoc-Glu-OtBu (150 mg, 0.354 mmol) and finally N^{10}-(trifluoroacetyl) pteroic acid (144 mg, 0.354 mmol) were coupled to the resin by repeating the above procedures. In the fifth step, a 2% hydrazine solution in DMF (3 × 5 ml) was added to the reaction vessel at room temperature for 2 h to remove the trifluoroacetyl group of pteroic acid. Next, 5 ml of a solution of TFA: H_2O: TIPS (95, 2.5: 2.5, *v*/v/v) was added to react for 2 h at room temperature to cleave the product from the resin and deprotect the tert-butyl and trityl groups [44]. Finally, the synthesized compound dissolved in TFA: H_2O: TIPS (95: 2.5: 2.5, v/v/v) was precipitated in 50 ml diethyl ether and collected by centrifugation. The precipitate was purified by washing three times with diethyl ether and dried under vacuum. The obtained compound was characterized by analytical UPLC and LC-MS as described in Section 2.2. Synthesis and characterization of non-folate control spacer $FmocP_5SH$ is described in the supplementary information (Supplementary section 1.1).

2.3.2. Synthesis of FA-PEG_{27}-SH ($FP_{27}S$)

The solid phase synthesis of FA-PEG_{27}-SH includes six steps which were similar to the synthesis of FA-PEG_5-SH. The only difference is the second step: coupling of Fmoc-NH-PEG_{27}-COOH instead of Fmoc-NH-PEG_5-COOH. The product was characterized by UPLC and LC-MS as described in Section 2.2.

2.3.3. Synthesis of FA-Asp-Arg-Asp-Asp-SH (FAS)

The solid phase synthesis of FA-peptide-SH includes nine steps. The peptide sequence was Asp-Arg-Asp-Asp-Cys. The coupling order to the resin was Fmoc-Cys(Trt)-OH, Fmoc-Asp(OtBu)-OH, Fmoc-Asp(OtBu)-

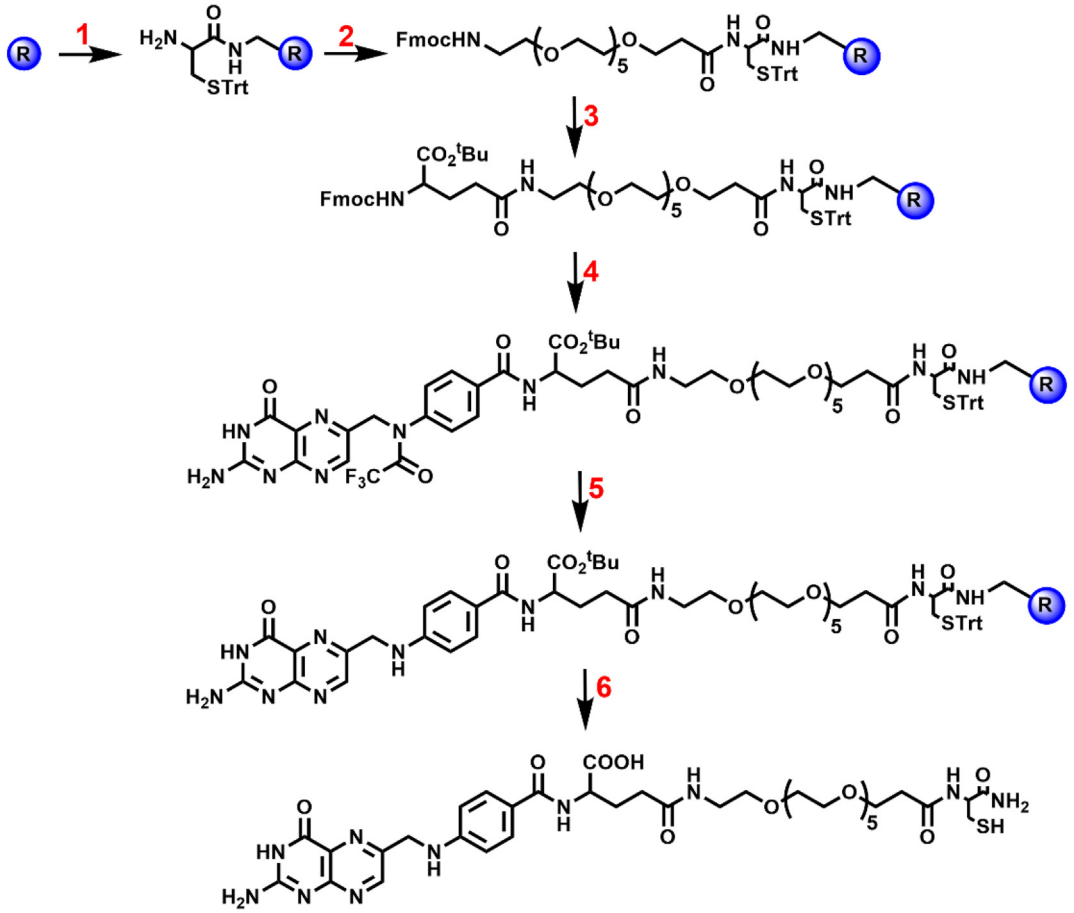

Fig. 2. Fluorenylmethylmethoxycarbonyl (Fmoc) solid phase peptide synthesis (SPPS) of FA-PEG_5-SH (FP_5S). R means Fmoc-2,4-dimethoxy-4′-(carboxymethyloxy)-benzhydrylamine aminomethyl resin. Reagents and conditions: (1) (i) 20% piperidine; (ii) Fmoc-Cys(Trt)-OH, BOP, DIPEA, 1 h; (iii) acetic anhydride, HOBt and DIPEA; (iv) 20% piperidine. (2) (i) Fmoc-NH-PEG_5-COOH, BOP, DIPEA, 12 h; (ii) acetic anhydride, HOBt and DIPEA; (iii) 20% piperidine. (3) (i) Fmoc-Glu-OtBu, BOP, DIPEA, 1 h; (ii) acetic anhydride, HOBt and DIPEA; (iii) 20% piperidine. (4) N^{10}-(trifluoroacetyl)pteroic acid, BOP, DIPEA, 12 h. (5) 2% hydrazine solution, (3 × 1 h). (6) TFA: H_2O: TIPS (95: 2.5: 2.5, *v*/v/v), 2 h.

OH, Fmoc-Arg(Pbf)-OH, Fmoc-Asp(OtBu)-OH again, Fmoc-Glu-OtBu and N^{10}-(trifluoroacetyl)pteroic acid. The final compound was cleaved from the resin using 5 ml TFA: H_2O: TIPS (95, 2.5: 2.5, *v*/v/v) mixture. The resulting mixture was concentrated to ~2 ml under reduced pressure and then dropwise added to ethyl ether to precipitate the product. Next, the precipitate was collected by centrifugation, washed with ethyl ether three times, and dried under vacuum. The product was characterized by analytical UPLC and LC-MS as described in Section 2.2.

2.4. Synthesis of Lx-dactolisib and Lx-lissamine

The synthesis scheme of Lx-dactolisib and Lx-lissamine is shown in Supplementary Fig. 1.

2.4.1. Synthesis of Lx-dactolisib

Dactolisib was coordinated to the platinum linker Lx using a similar method as previously reported for other drug containing nitrogen functional groups [45–47]. Briefly, [PtCl(ethylenediamine)NO_3] was synthesized by reacting [$PtCl_2$(en)] (750 mg, 2.307 mmol) with $AgNO_3$ (390 mg, 1 equiv) in 15 ml DMF overnight in the dark at room temperature. The formed silver chloride precipitate was removed by filtration through a PTFE filter (0.2 μm, 47 mm diameter, Whatman). Subsequently, dactolisib (400 mg, 0.848 mmol) was dissolved in 10 ml DMF at 75 °C, after which, activated Lx solution (5.64 ml, 1 equiv) in DMF was added to the dactolisib solution and reacted at 60 °C for 24 h. The formed Lx-dactolisib complex was isolated using Waters preparative HPLC system (Section 2.2). The fractions that contained the aimed product (UPLC and LC-MS analysis) were pooled and freeze-dried. ^{1}H NMR spectroscopic analysis was used to identify which aromatic nitrogen of dactolisib was coordinated to the platinum linker Lx.

2.4.2. Synthesis of Lx-lissamine

Lx-lissamine was synthesized in two steps. Firstly, imidazole was reacted with lissamine sulfonyl chloride to obtain imidazole-lissamine [48]. Secondly, imidazole-lissamine was reacted with activated Lx to obtain Lx-lissamine (Supplementary Fig. 1C). For the synthesis of imidazole-lissamine (IMI-lissamine), 3-(1H-imidazol-1-yl)propan-1-amine (204 mg, 1.63 mmol) and triethylamine (0.378 ml, 2.71 mmol) were sequentially added to a solution of lissamine B sulfonyl chloride (783 mg, 1.36 mmol) in dry CH_2Cl_2 (30 ml) at 0 °C. After 5 min, the reaction mixture was allowed to warm to room temperature and stirred for 40 h. Subsequently, the solution was diluted with 30 ml dichloromethane (DCM) and washed with an aqueous solution of saturated $NaHCO_3$, water, brine, and dried with Na_2SO_4, filtered, and concentrated. The crude product was purified by preparative HPLC as described in Section 2.2. The fractions that contained the aimed product (UPLC and LC-MS analysis) were pooled and freeze-dried. For the synthesis of Lx-lissamine, IMI-lissamine (100 mg, 0.150 mmol) dissolved in 10 ml DMF was added to a solution of activated Lx (998 μl, 0.150 mmol) and the mixture was stirred at room temperature for 24 h in the dark. The reaction solution was subsequently loaded onto a preparative HPLC column and fractionated as described in Section 2.2.

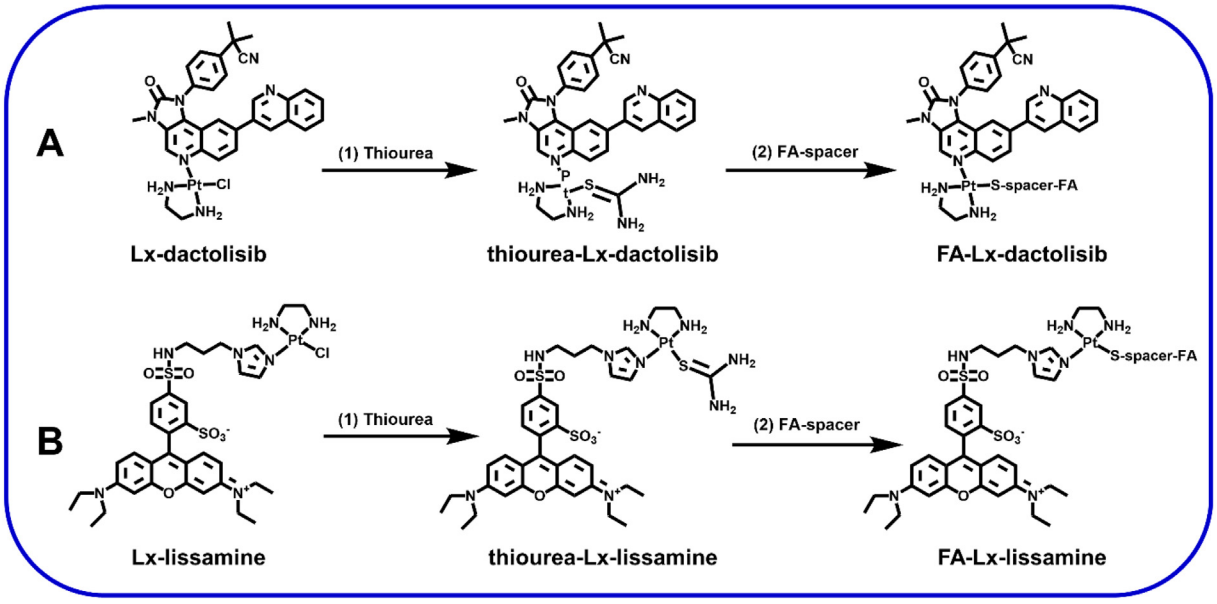

Fig. 3. Synthesis of the FA-Lx-dactolisib and FA-Lx-lissamine conjugates. (A) Lx-dactolisib was reacted with thiourea, and subsequently the cysteine containing FA-spacer adducts were reacted with thiourea-Lx-dactolisib to yield the FA-Lx-dactolisib conjugates. (B) The same synthesis route for FA-Lx-lissamine.

The fractions that contained the aimed product were collected and freeze-dried. The purity of synthesized Lx-lissamine was analyzed by UPLC and the structure was confirmed by LC-MS analysis as described in Section 2.2. The detection wavelength was 560 nm.

2.5. Synthesis of FA-Lx-dactolisib and FA-Lx-lissamine conjugates

Lx-dactolisib and Lx-lissamine were firstly reacted with thiourea to form intermediate adducts thiourea-Lx-dactolisib and thiourea-Lx-lissamine (Fig. 3). In a subsequent step, the formed thiourea adducts were reacted with the three FA-spacer adducts (FP_5S, $FP_{27}S$ and FAS, synthesized as described in Section 2.3) to yield the final FA-Lx-dactolisib and FA-Lx-lissamine conjugates. In brief, thiourea (5.5 mg, 0.072 mmol) was reacted with an equimolar amount of Lx-dactolisib (54.7 mg, 0.072 mmol) or Lx-lissamine (68.8 mg, 0.072 mmol) respectively in 15 ml 20 mM tricine/$NaNO_3$ buffer (pH 8.5) for 16 h at room temperature in the dark. Subsequently, the formed thiourea-Lx-dactolisib and thiourea-Lx-lissamine were reacted with an equimolar amount of FP_5S, $FP_{27}S$ or FAS respectively in 10 ml 20 mM tricine/$NaNO_3$ buffer 1:2 (*v*/v) for 24 h at room temperature in the dark. Six targeted conjugates were synthesized in total (Table 1). The six reaction solutions were separately loaded onto a preparative HPLC column to collect the fractions with the aimed products as described in Section 2.2. The collected fractions with the products were subsequently pooled and freeze-dried. The purity of the synthesized conjugates was analyzed by UPLC and the structure of the conjugates was confirmed by LC-MS analysis as described in Section 2.2. The detection wavelength was 340 nm for FA-Lx-dactolisib and 560 nm for the FA-Lx-lissamine conjugates. In addition to the folate-Lx-lissamine conjugates listed above, non-folate control conjugate was prepared by reacting $FmocP_5SH$ with Lx-lissamine. Characterization of $FmocP_5SH$ and $FmocP_5S$-Lx-lissamine is described in the supplementary information (Supplementary Fig. 2).

Table 1
Yields and LC-MS characterization of the synthesized compounds.

Categories	Compounds	Yield (%)	LC-MS (ESI)
FA-spacer	FP_5S	60	$(M + H)^+$ 879.6
	$FP_{27}S$	60	$(M + H)^+$ 1848.3
	FAS	63	$(M + H)^+$ 1045.7
Lx-drug/dye	Lx-dactolisib	21	$(M)^+$ 759.6
	Lx-lissamine	40	$(M)^+$ 955.2
FA-Lx-dactolisib	FP_5S-Lx-dactolisib	77	$(M)^+$ 1602.4
	$FP_{27}S$-Lx-dactolisib	74	$(M + H)^{2+}$ 1286.0
	FAS-Lx-dactolisib	69	$(M)^+$ 1768.7, $(M + H)^{2+}$ 884.8
FA-Lx-lissamine	FP_5S-Lx-lissamine	81	$(M)^+$ 1798.6, $(M + H)^{2+}$ 899.8
	$FP_{27}S$-Lx-lissamine	80	$(M + H)^{2+}$ 1384.1
	FAS-Lx-lissamine	67	$(M + H)^{2+}$ 982.8

2.6. Drug release profiles of FA-Lx-dactolisib conjugates

The biological stability and drug release properties of FA-Lx-dactolisib were studied by incubating FP_5S-Lx-dactolisib, $FP_{27}S$-Lx-dactolisib and FAS-Lx-dactolisib (final concentration: 50 μM) at 37 °C in different media: fetal calf serum (FCS), cell culture medium, PBS with 10 mM glutathione (GSH) and PBS with 10 mM dithiothreitol (DTT). Small aliquots (100 μl) were taken after 3, 6 and 24 h of incubation and used for analysis of released dactolisib. The total amount of reversibly conjugated dactolisib was quantified by overnight incubation with 0.5 M KSCN in PBS at 80 °C [49]. Since dactolisib has a limited aqueous solubility (log *P* = 5.2 [38]), two volumes of acetonitrile were added to solubilize the released drug. The samples were vortexed and centrifuged and 5 μl of the supernatant was injected for UPLC analysis to quantify the amount of released dactolisib as described in Section 2.2. Calibration was done using dactolisib standards in acetonitrile in a concentration range of 0.15 to 50 μg/ml (injection volume 5 μl) to calculate the concentrations in the different samples.

2.7. Cell culture

The human kidney tubular epithelial cell line (HK−2) and human adenocarcinoma alveolar based lung cancer cell line (A549) were obtained from the American Type Culture Collection (ATCC, Manassas, Virginia, USA). HK-2 cells are folate receptor positive (FR^+) whereas A549 cells are folate receptor negative (FR^-). HK-2 cells were cultured in folic acid free Dulbecco's modified Eagle's medium (DMEM) containing 3.7 g/l sodium bicarbonate, 1.0 g/l glucose and supplemented with 10% (*v*/v) fetal calf serum (FCS), penicillin (100 IU/ml),

streptomycin (100 μg/ml) and amphotericin B (0.25 μg/ml) at 37 °C with 5% CO_2 in humidified air. A549 cells were cultured in DMEM-HAM's F12 medium supplemented with 10% (v/v) fetal calf serum (FCS) and 1% penicillin/streptomycin at 37 °C in an incubator with 5% CO_2 and humidified atmosphere. Both HK-2 and A549 cells were grown in 25 cm^2 cell culture flasks and passaged twice a week.

2.8. Kinase inhibitory effect of FA-Lx-dactolisib conjugates in HK-2 cells

A western blotting assay was used to evaluate whether FA-Lx-dactolisib conjugates can inhibit the mTOR and PI3K pathways in cells. The activity of the mTOR pathway was investigated with a phospho-S6 ribosomal protein (Ser240/244) rabbit antibody, while the activity of the PI3K pathway was studied using a phospho-Akt (Ser473) rabbit antibody [50]. HK-2 cells were seeded (2×10^5 cells/well) into 6-well plates and subsequently cultured for 2 days. Next, 1 mM stock solutions of the FP_5S-Lx-dactolisib, FP_{27}S-Lx-dactolisib, FAS-Lx-dactolisib conjugates as well as dactolisib in DMSO were diluted to 500 nM with culture medium supplemented with 10% (*v*/v) fetal calf serum (FCS). Next, the cells were cultured for 24 h and lysed using RIPA buffer supplemented with protease and phosphatase inhibitors. The proteins P-S6 and P-Akt in the lysate were separated by SDS-polyacrylamide gel electrophoresis on NuPAGE 4–12% Bis-Tris protein gels (4–12%) [51]. The proteins were subsequently transferred onto a nitrocellulose membrane using the iBlot dry blotting method. The membranes were blocked with TBS-T [Tris-buffered saline, 0.1% Tween 20, 20 mM tris (pH 7.6), 150 mM NaCl and 0.1% Tween 20] for 1 h at room temperature and incubated with the primary antibodies β-Actin rabbit mAb, phospho-S6 ribosomal protein (Ser240/244) rabbit antibody and phospho-Akt (Ser473) rabbit mAb overnight at 4 °C. The membranes were washed three times with TBS-T and incubated with horseradish peroxidase (HRP)-conjugated goat anti-rabbit secondary antibody for 1 h at room temperature. Proteins were visualized by a chemiluminescence-based detection reagent and the protein bands were quantified on a Gel Doc Imaging system equipped with a XRS camera [36]. In addition, folate competition experiments were conducted by incubation of the cells with medium containing 500 μM folic acid (i.e. 1000-fold excess) for 30 min before the conjugates were added.

2.9. Cellular uptake of FA-Lx-lissamine conjugates

FA-Lx-lissamine conjugates were used to study the cellular uptake of the conjugates by confocal fluorescence microscopical analysis. HK-2 cells (FR^+) and A549 cells (FR^-) in culture medium were seeded (1×10^4 cells/well) into 96-well plates and incubated for 24 h. Next, 1 mM stock solutions of the FP_5S-Lx-lissamine, FP_{27}S-Lx-lissamine and FAS-Lx-lissamine conjugates in DMSO were diluted to 10 μM with culture medium supplemented with 10% (*v*/v) fetal calf serum (FCS) before the solutions were added to the wells. Cells were incubated with the conjugates for 2 h at 37 °C [52]. Next, 5 μl Hoechst 33342 (1:1000 dilution in PBS) was pipetted into the wells and the cells were incubated for 30 min to stain their nuclei. The cells were washed 3 times with PBS to remove non-bound conjugates. Confocal images were acquired on a fully automated Yokogawa High Content Imaging Platform (Model CV7000, Yokogawa, Tokyo, Japan) using a 60× oil objective at 445 nm, 525 nm and 600 nm channels. In addition, the specific uptake of FA-Lx-lissamine conjugates by HK-2 cells was investigated in a competitive uptake inhibition assay, where the cells were incubated with medium containing 1000 μM folic acid (i.e. 100-fold excess) for 30 min before the conjugates were added.

2.10. Biodistribution of FA-Lx-lissamine conjugates and immunohistochemical analysis

Animal experiments were approved by the animal experimental committee of Leiden University, The Netherlands. Organ distribution and kidney accumulation of FA-Lx-lissamine conjugates were studied in kidney specific *Pkd1* deletion mice (iKsp-$Pkd1^{del}$) [22,53]. iKsp-$Pkd1^{del}$ mice were maintained on a standard 12 h light-dark cycle and fed ad libitum. Pkd1 deletion was induced by administering tamoxifen (150 mg/kg in sunflower oil) via oral gavage at post-natal day 18 and 19. Starting from 7 weeks after injecting tamoxifen, renal function was monitored by measuring blood urea (BU) concentration on a weekly basis on 30 μl blood samples from the tail vein. The onset of renal failure, at which the mice have severe PKD, was defined as having BU > 20 mmol/l, which was typically reached at an age range from 14 to 16 weeks. Administration of conjugates and harvesting of organs were carried out as previously reported for intrarenal accumulation of folate-DTPA conjugates [54]. Single mice with advanced stage of PKD were injected intraperitoneally (i.p.) with either FP_5S-Lx-lissamine, FP_{27}S-Lx-lissamine, FAS-Lx-lissamine or $FmocP_5$S-Lx-lissamine (non-folate control) at a dose of 2 μmol/kg dissolved in PBS. The injection volume was 200 μl. A mouse injected with 200 μl PBS was used as vehicle control. 1.5 h post administration of conjugates, the mice were euthanized by cervical dislocation and kidneys, liver and spleen were harvested and rinsed with saline. Small pieces of the organs (1 to 2 mm thick) were covered with TissueTek OCT, rapidly frozen in liquid nitrogen and stored at −80 °C until further processing. Cryosections (5 μm thick, Leica CM3050 Cryostat) were fixed in 100 ml methanol for 10 min and counterstained with Hoechst 33342 nuclear dye (1.0 μg/ml) for 10 min. The sections were washed with PBS and mounted using FluorSave™ Reagent. Finally, the stained sections were analyzed using Keyence BZ-9000 microscopy fluorescent microscope. The colocalization of the conjugates with folate receptors in kidney sections was investigated using rabbit anti-folate primary antibody (dilution 1:20) by overnight staining at 4 °C followed by secondary with donkey anti-rabbit IgG (H + L) Alexa Fluor 488 secondary antibody (dilution 1:200) at room temperature for 2 h [55]. Antibodies were diluted in PBS with 1% bovine serum albumin and 1% sodium azide. Kidney sections were washed with PBS containing 0.05% Tween-20 (PBST) three times after each staining step.

2.11. Statistical analysis

GraphPad Prism software version 6 (GraphPad Software, Inc.) was used for statistical analysis. The analyses were performed using the unpaired two-tailed Student's *t*-test. The experimental data are presented as means ± SEM. Statistical significance was considered when the *P* value was 0.05.

3. Results and discussion

3.1. Synthesis and characterizations of FA-Lx-dactolisib and FA-Lx-lissamine conjugates

As pointed out in the Introduction, dactolisib lacks common functional groups for covalent conjugation to folate or spacer moieties, and therefore a strategy was employed in which the drug was coupled via platinum(II) coordination chemistry to a FA-spacer adduct. As fluorescent controls, lissamine conjugates were synthesized via a similar linker approach and used to study uptake in kidney cells and organ distribution. The developed synthetic route consists of three steps: 1. the synthesis of three FA-spacer adducts (FP_5S, FP_{27}S and FAS); 2. the synthesis of Lx-dactolisib and Lx-lissamine; 3. the coupling of the FA-spacer adduct to Lx-dactolisib and Lx-lissamine (Fig. 3).

3.1.1. Synthesis and characterization of the FA-spacer adducts

In many studies, folate has been modified using carbodiimide coupling reagents [56–58]. However, both the α- and γ-carboxylic group of folate can be activated using this method yielding only partially functional conjugates, since the α-carboxylic group of folate is essential for binding to FR [59–61]. This means that the γ-COOH of folate should be

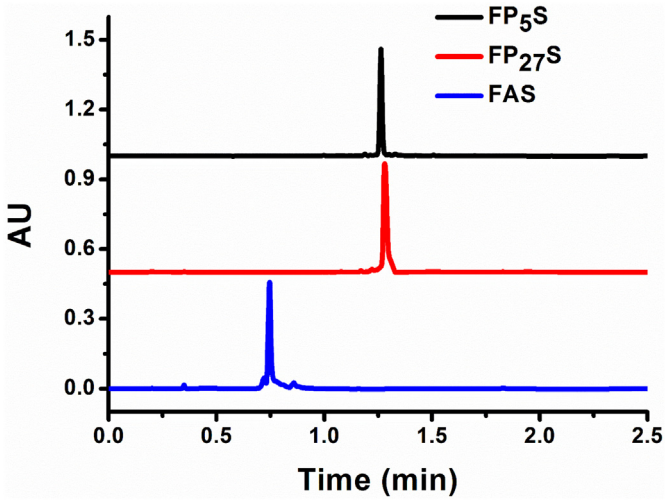

Fig. 4. UPLC analysis of the different FA-spacer compounds. The detection wavelength was 290 nm. The retention times for FP_5S, $FP_{27}S$ and FAS was 1.2 min, 1.3 min and 0.7 min respectively. The purity (based on AUC) was > 95%.

exploited exclusively for conjugation reactions, leaving the other COOH group unaffected and thus able to maintain the binding and uptake in target cells. Therefore, fluorenylmethylmethoxycarbonyl (Fmoc) solid phase peptide synthesis (SPPS) was used to obtain the regioselective FA-spacer adducts in which the spacers were only coupled to the γ-carboxyl group of folate [62–64]. In this method, folic acid was formed by coupling pteroic acid with glutamic acid of which its α-COOH was protected with a tert-butoxy group (Fig. 2) [65]. In a subsequent step, the γ-COOH of folate was used for conjugation with the spacers [59]. PEG_5-Cys, PEG_{27}-Cys and Asp-Arg-Asp-Asp-Cys peptide were chosen as spacers to increase the hydrophilicity and thus the aqueous solubility of the final conjugates. UPLC chromatograms of the purified compounds showed main peaks for the target products with some small impurities (Fig. 4). FP_5S, $FP_{27}S$ and FAS were obtained with ~60% yield (Table 1). The identity of the different synthesized FA-spacer adducts was confirmed by LC-MS (Table 1); the *m/z* of the peaks is in agreement with the molecular weight of the compounds as detected by LC-MS analysis (Supplementary Fig. 3).

3.1.2. Synthesis and characterizations of Lx-dactolisib and Lx-lissamine

To obtain the Lx-drug/dye complexes, the Lx linker was firstly activated with $AgNO_3$. The activated Lx linker was subsequently coupled to dactolisib and IMI-lissamine (an imidazole-derivative of lissamine which also reacts to Lx via coordination chemistry [34]) to obtain the Lx-dactolisib and Lx-lissamine complexes (Supplementary Fig. 1). The molar feed ratio of activated Lx to dactolisib or IMI-lissamine was 1:1 and the crude products were purified by preparative HPLC. All compounds were obtained in yields in a range between 21% and 39% and high purity (Table 1). Dactolisib is an imidazoquinoline structure modified with a quinoline group, both quinolines can in principle coordinate with Lx linker to form platinum-coordination complexes. The UPLC analysis of the crude reaction mixture of dactolisib with activated Lx in 1:1 ratio is shown in Supplementary Fig. 4A. Besides the starting compound, three major product peaks were observed, either corresponding to conjugates in which a single Lx has been coupled to dactolisib, or to the 2:1 Lx:dactolisib conjugate as was demonstrated by LC-MS of the reaction mixture (Supplementary Fig. 4B). The most abundant reaction complex (peak 3) was purified from the mixture solution using preparative HPLC to obtain the Lx-dactolisib complex further used in the studies. The identity and conjugation site of the isolated complex was confirmed by ^{1}H NMR via comparison of the spectra of Lx-dactolisib and dactolisib (Fig. 5). For dactolisib and Lx-dactolisib, the proton labeled “a” (8.78 ppm (d, J = 2.4 Hz, 1H)) and the proton labeled “b” (8.39 ppm (d, J = 2.4 Hz, 1H)) are at the same position in the NMR spectra, demonstrating that the linker Lx is not coordinated to the aromatic nitrogen labeled “1”. On the contrary, the proton labeled “e” (9.05 ppm (s, 1H)), the proton labeled “c” (8.20 ppm (d, J = 8.8 Hz, 1H)) and the proton labeled “d” (8.10 ppm (dd, J = 8.9, 2.1 Hz, 1H)) of dactolisib shifted to 9.55 ppm (s, 1H), 9.74 ppm (d, J = 9.2 Hz, 1H) and 8.38 ppm (dd, J = 9.2, 2.1 Hz, 1H) after coordination of the linker, demonstrating that the linker Lx is coordinated to the aromatic nitrogen labeled “2”. The purity and identity of the obtained Lx-dactolisib and Lx-lissamine was furthermore confirmed by UPLC and LC-MS analysis, respectively (Supplementary Fig. 5). The insert of Supplementary Fig. 5 shows the characteristic isotope distribution of the four stable isotopes of platinum (^{194}Pt, ^{195}Pt, ^{196}Pt, ^{198}Pt: 32.9, 33.8, 25.3, 7.2%), which confirms the identities of the isolated bioinorganic platinum complexes [66].

3.1.3. Synthesis and characterization of FA-Lx-dactolisib and FA-Lx-lissamine conjugates

FA-spacer adducts (FP_5S, $FP_{27}S$ and FAS) were coupled to Lx-dactolisib and Lx-lissamine to form FA-Lx-dactolisib and FA-Lx-lissamine conjugates. To avoid coordination of the Lx linker to aromatic nitrogens in drug or FA, Lx-dactolisib and Lx-lissamine were first reacted with thiourea to yield the intermediate compounds thiourea-Lx-dactolisib and thiourea-Lx-lissamine (Fig. 3). Since thiourea forms relative stable coordination complexes with platinum (i.e. relative to platinum(II) complexes formed with chloride or water), the thiourea intermediate compounds will not react readily with aromatic nitrogens but are still able to react with the thiol group of the FA-spacer adducts [34,67]. In total, six conjugates were synthesized: FP_5S-Lx-dactolisib, $FP_{27}S$-Lx-dactolisib, FAS-Lx-dactolisib, FP_5S-Lx-lissamine, $FP_{27}S$-Lx-lissamine and FAS-Lx-lissamine. After purification by preparative HPLC, the conjugates were obtained in yields in a range between 67% and 81% (Table 1). The purity (> 95%) and identity of synthesized conjugates was established by UPLC analysis (Fig. 6) and LC-MS analysis (Supplementary Figs. 6 and 7), respectively.

3.2. Drug release characteristics of FA-Lx-dactolisib conjugates

The stability and drug release behavior of the three FA-Lx-dactolisib conjugates: FP_5S-Lx-dactolisib, $FP_{27}S$-Lx-dactolisib and FAS-Lx-dactolisib were studied by incubating them at 37 °C in different media: fetal calf serum (FCS), cell culture medium, 10 mM glutathione (GSH) in PBS and 10 mM dithiothreitol (DTT) in PBS. These two latter reagents were chosen for their behavior as coordinative ligands for platinum(II) rather than as reducing agents. GSH and other thiols or sulfur containing reagents can release N-heterocyclic drugs from Lx by competitive displacement, as has been demonstrated previously for other platinum(II)-drug complexes [34,68]. Fig. 7 shows that 5% and 8% parent dactolisib was released from FP_5S-Lx-dactolisib after 24 h incubation in serum and culture medium, respectively. Similar amounts of drug were released from $FP_{27}S$-Lx-dactolisib and FAS-Lx-dactolisib after 24 h incubation in serum and culture medium (5–7%). This demonstrates that the conjugates had a good stability in normal media. In contrast, 18% and 66% dactolisib was released from FP_5S-Lx-dactolisib after 24 h incubation in medium containing GSH and DTT respectively, whereas 23% and 80% dactolisib was released from $FP_{27}S$-Lx-dactolisib after 24 h incubation in medium with GSH and DTT respectively. The drug released from FAS-Lx-dactolisib after 24 h incubation in medium containing GSH and DTT was 19% and 70% respectively. The extent of drug release in medium with DTT was more than in medium with GSH, which is in agreement with the previous studies [49,69]. DTT has two thiol groups while GSH only has one. The stronger reducing character of DTT furthermore prevents its oxidation in the medium during the 24 h incubation, while GSH will be oxidized to GSSG during the time course of the experiment. These differences explain the higher extent of release in

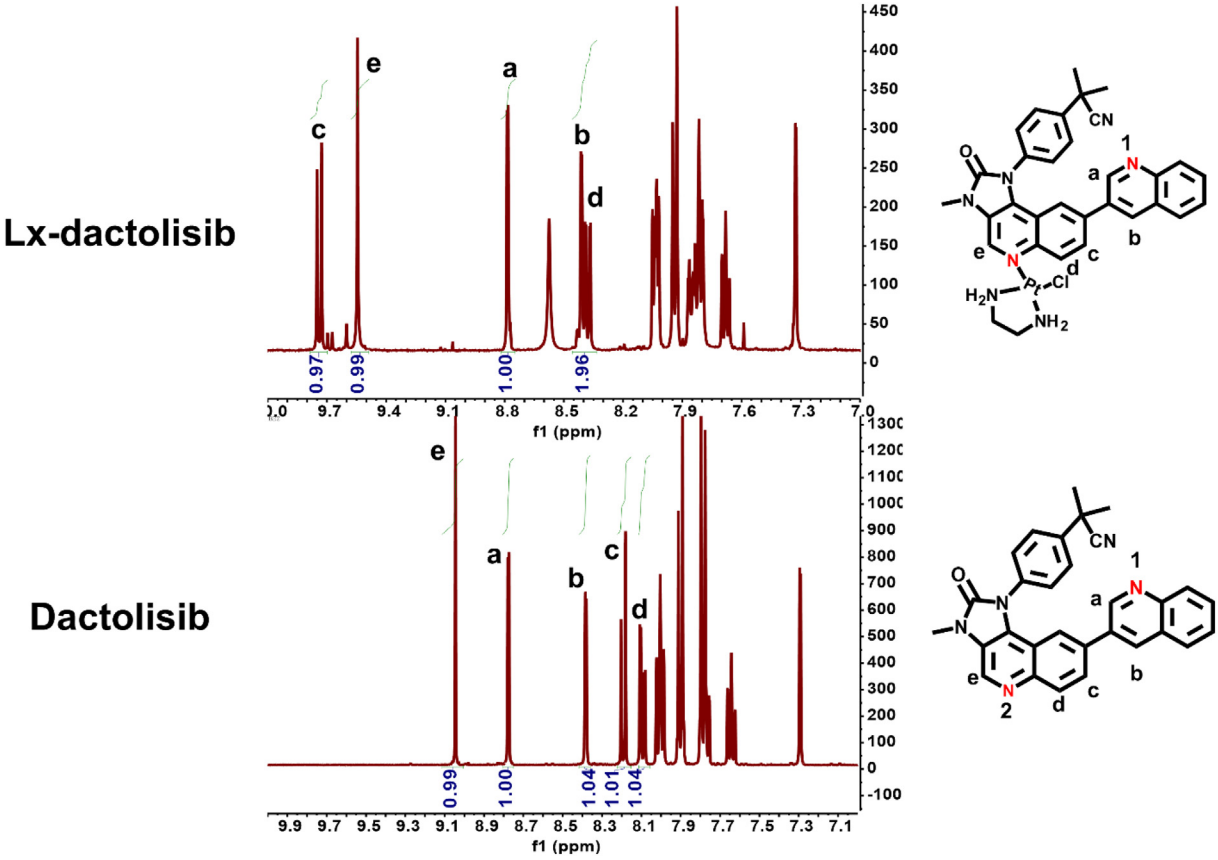

Fig. 5. Expansion of ^{1}H NMR spectra of dactolisib and Lx-dactolisib in DMSO-d_6 in the 7–10 ppm region. The integrations of characteristic protons are labeled on the spectra. Full spectra (0–10 ppm) are shown in Supplementary Fig. 4C.

presence of DTT, although GSH driven release probably better reflects intracellular conditions. Slow intracellular release was also observed upon in vivo administration, as for instance was observed for the kidney-targeted conjugate SB202190-lysozyme [68]. Our present result as shown in Fig. 7 confirm that dactolisib can be released from the conjugates via competitive displacement with sulfur donors. Moreover, Fig. 7 also shows that the release kinetics of dactolisib from the conjugates is independent of the type of spacer.

3.3. Kinase inhibitory effect of FA-Lx-dactolisib conjugates on HK-2 cells

The kinase inhibitory effect of the three FA-Lx-dactolisib conjugates was studied in HK-2 cells by determination of the phosphorylation levels of the signaling pathways downstream of PI3K and mTOR, i.e. phospho-Akt and phospho-S6, respectively. Fig. 8 shows that dactolisib significantly inhibited the phosphorylation of Ser240/244-S6 and Ser473-Akt in HK-2 cells. Incubation of the cells with FP_5S-Lx-dactolisib, FP_{27}S-Lx-dactolisib and FAS-Lx-dactolisib conjugates also significantly reduced the phosphorylation of Ser473-Akt and Ser240/244-S6 at nanomolar concentrations. The pharmacological activity of FP_5S-Lx-dactolisib, FP_{27}S-Lx-dactolisib and FAS-Lx-dactolisib was almost the same as free dactolisib. Importantly, the kinase inhibitory effect of the three FA-Lx-dactolisib conjugates could be blocked by 500 μM folate, i.e. a 1000-fold excess over the concentration of FA-Lx-dactolisib

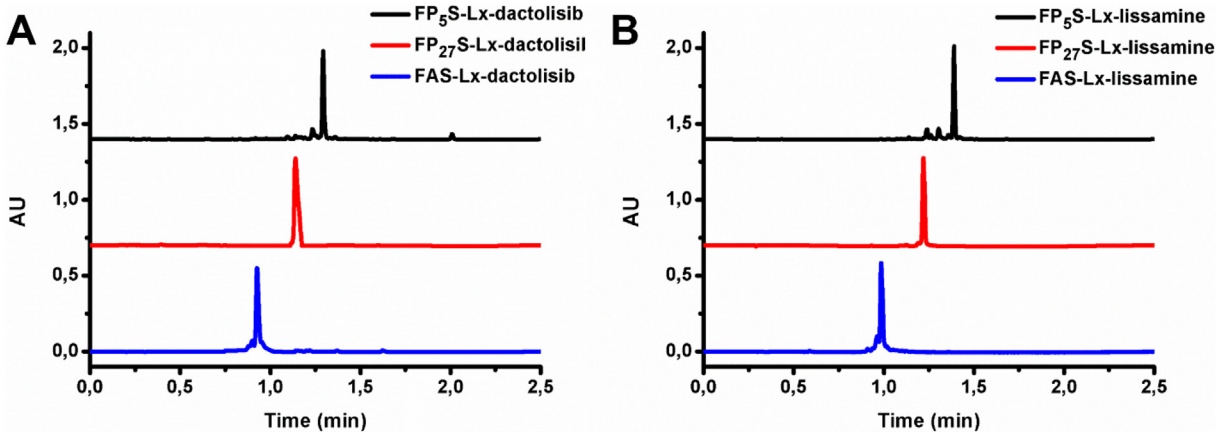

Fig. 6. (A) UPLC chromatograms of FA-Lx-dactolisib conjugates. The detection wavelength was 340 nm. (B) UPLC chromatograms of FA-Lx-lissamine conjugates. The detection wavelength was 560 nm.

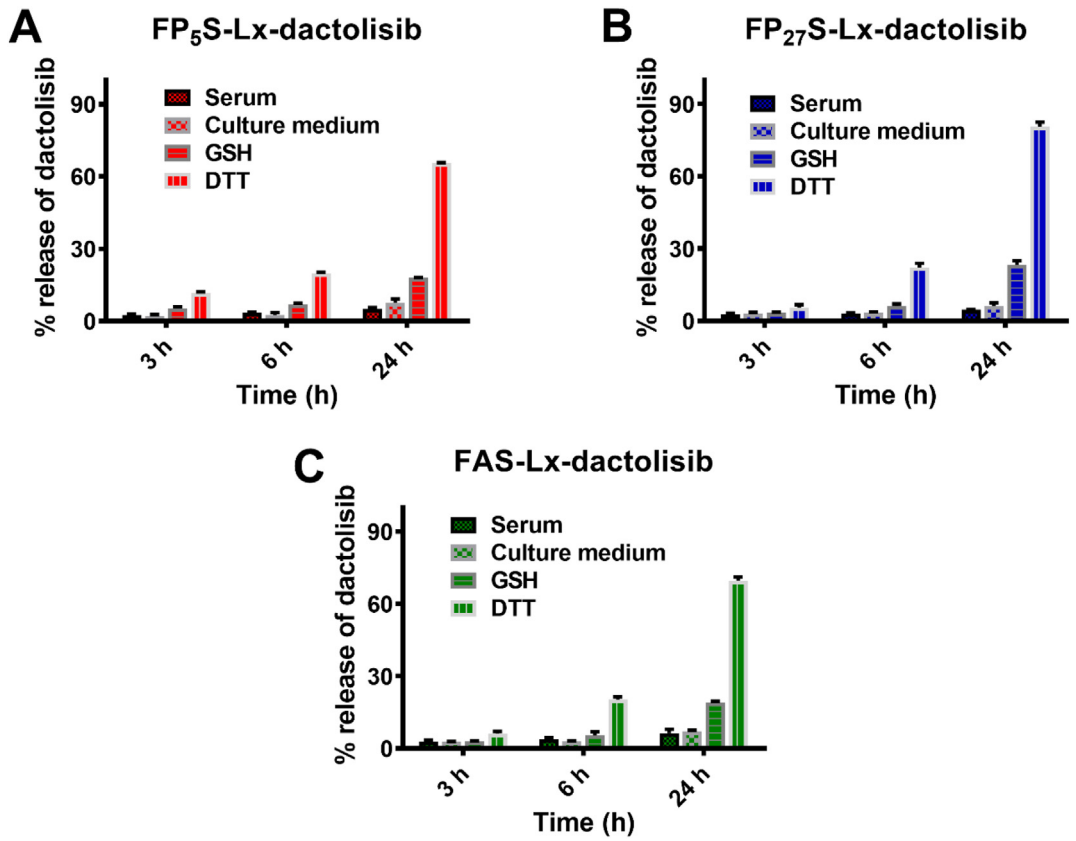

Fig. 7. Drug release profiles of FA-Lx-dactolisib conjugates upon incubation for 3, 6 and 24 h at 37 °C in fetal calf serum, culture medium, medium with 10 mM GSH and medium with 10 mM DTT. Released drug was related to the amount of coupled dactolisib as determined by the KSCN displacement assay (Section 2.6). (A) Drug release profiles of FP_5S-Lx-dactolisib. (B) Drug release profiles of $FP_{27}S$-Lx-dactolisib. (C) Drug release profiles of FAS-Lx-dactolisib.

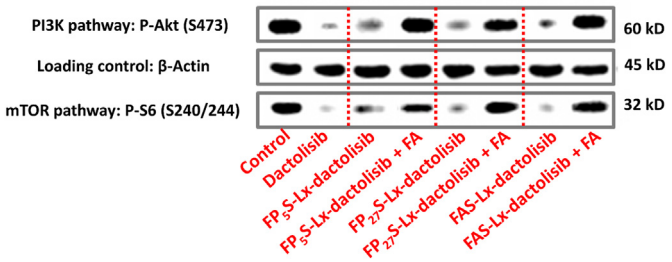

Fig. 8. Western blot analysis of phosphorylation of Ser240/244-S6 and Ser473-Akt in HK-2 cells treated with 500 nM dactolisib, FP_5S-Lx-dactolisib, $FP_{27}S$-Lx-dactolisib and FAS-Lx-dactolisib conjugates with or without 500 μM folate for 24 h at 37 °C. β-Actin was used as a loading control.

conjugates (Fig. 8). Such a high concentration of folate had no toxic effects on HK-2 cells nor did it affect the phosphorylation of Ser473-Akt and Ser240/244-S6 (Supplementary Fig. 8). The absence of inhibitory activity of all three conjugates in presence of excess folate demonstrates that these conjugates cannot enter the cells passively, which makes their cellular specificity quite different from the parent dactolisib compound. The activity of FA-Lx-dactolisib conjugates is restricted to cells that internalize the conjugates receptor-mediated endocytosis via FR. Since the conjugates cannot cross over cell membranes nor membranes of endocytic vesicles (e.g. endosomes or lysosomes), it is unlikely that FA-Lx-dactolisib conjugates can exert kinase inhibitory effects directly. Intracellular release of dactolisib from the conjugates thus must have provided sufficient amounts of free drug within the timeframe of the experiments.

3.4. Cellular uptake studies of FA-Lx-lissamine conjugates

Internalization of FA-Lx-lissamine conjugates by FR^+ kidney epithelial cells (HK-2 cells) was studied by confocal fluorescence microscopy. FR^- cells (A549 cells) were used to exclude FR-independent uptake of conjugates. Strong intracellular fluorescence of lissamine was observed when HK-2 cells were incubated with the three FA-Lx-lissamine conjugates (Fig. 9A). The images clearly revealed that the conjugates were localized intracellularly in perinuclear vesicles of HK-2 cells, most likely lysosomes [70]. Fig. 9B shows the mean fluorescence intensities (MFI) calculated from the confocal images in Fig. 9A, showing that the cell-associated fluorescence of $FP_{27}S$-Lx-lissamine was highest as compared to the other two conjugates. The observed difference may relate to the higher hydrophilicity of the longer PEG-linker, resulting in better solvation of the folate ligand and its exposure to its counterreceptor FR. Folate conjugates were barely taken up by FR-negative cells (A549 cells), demonstrating that uptake by passive membrane transport into the cytosol is not occurring, thus restricting intracellular distribution of the conjugates to FR-expressing cells only. To further verify specificity of FR in the cellular uptake process, a competitive experiment with 100-fold excess of free folate was conducted (i.e. 1000 μM free folate, which is the highest concentration in view of its solubility in the medium). Fig. 9 shows strongly reduced uptake of all three conjugates in presence of excess folate. These immunofluorescence pictures show that the remaining uptake was still in a vesicular pattern. The relative lower fold-excess of folate (100-fold) in the present experiment is a plausible explanation for incomplete inhibition of receptor-mediated uptake. Taken together, these results demonstrate FR dependent uptake, subsequent intracellular processing endocytic vesicles and further intracellular inhibition of the signaling pathways targeted by dactolisib.

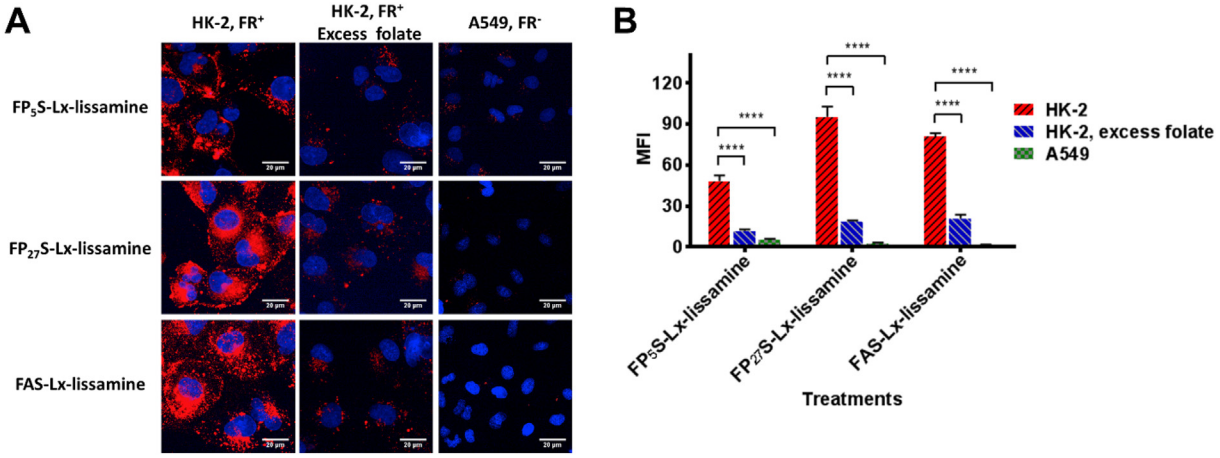

Fig. 9. Internalization of three targeted FA-Lx-lissamine conjugates by HK-2 and A549 cells. (A) Confocal microscopic images of HK-2 cells incubated with 10 μM FP_5S-Lx-lissamine, FP_{27}S-Lx-lissamine and FAS-Lx-lissamine conjugates with/without folic acid (1000 μM) and confocal microscopic images of A549 cells incubated with the same conjugates for 2 h at 37 °C. The internalized conjugates were shown in red color. Nuclei of cells were stained with Hoechst 33342 and displayed in blue color. (B) The corresponding mean fluorescence intensity (MFI) calculated from the confocal images, bars 20 μm, $P < 0.05$. (For interpretation of the references to color in this figure legend, the reader is referred to the web version of this article.)

3.5. Biodistribution of FA-Lx-lissamine conjugates in PKD mice

In order to demonstrate the feasibility of FA-Lx-lissamine conjugates for kidney targeting in polycystic kidney disease, 14 to 16-week old iKsp-*Pkd1*^{del} mice were injected with FA-Lx-lissamine conjugates intraperitoneally and sacrificed 1.5 h post injection, at which timepoint such small-folate conjugates have been largely taken up in the circulation from the intraperitoneal cavity and subsequently filtered and accumulated in the kidneys, as demonstrated previously with other folate conjugates [7,43]. Fig. 10 displays the fluorescence images of the kidneys, liver and spleen sections. FP_5S-Lx-lissamine, FP_{27}S-Lx-lissamine and FAS-Lx-lissamine conjugates which all contain the folate targeting moiety strongly accumulated in polycystic kidney tissue, while only low background fluorescence was observed in liver and spleen. Thus, after being administered intraperitoneally, folate targeted conjugates were indeed absorbed in the kidneys, even in animals suffering from an advanced stage of polycystic kidney disease. Moreover, the biodistribution study also shows that these folate conjugates have avoided uptake in other organs besides the kidneys. On the contrary, no kidney accumulation was observed in the control group which was injected with $FmocP_5$S-Lx-lissamine (conjugate without targeting ligand folate).

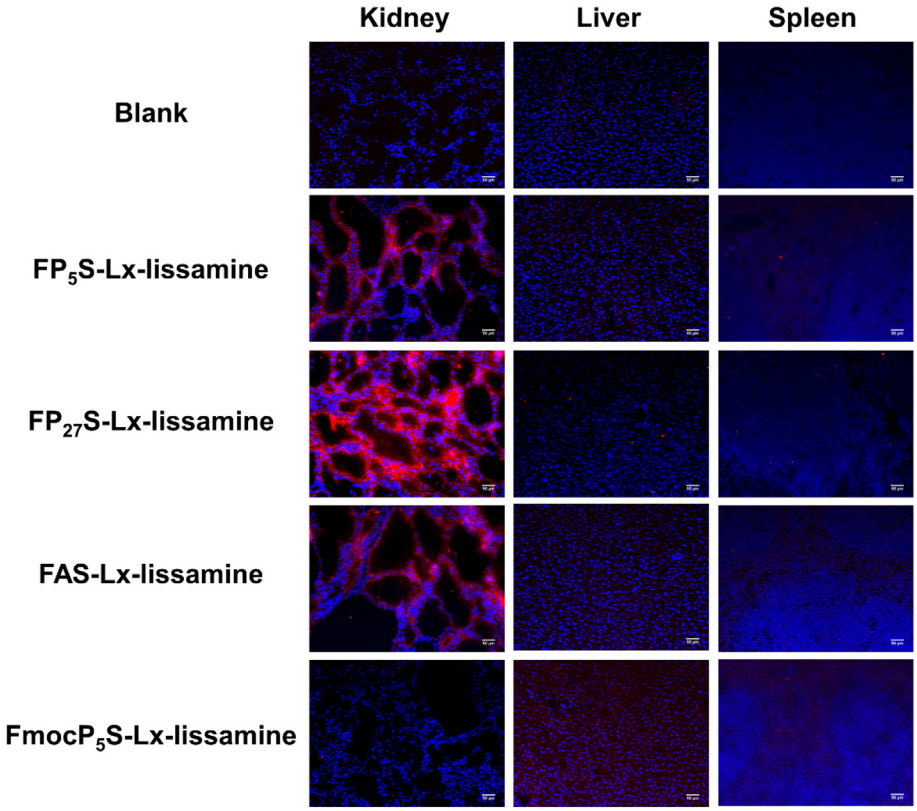

Fig. 10. Organ distribution of folate targeted conjugates (FP_5S-Lx-lissamine, FP_{27}S-Lx-lissamine and FAS-Lx-lissamine) and no folate ligand control $FmocP_5$S-Lx-lissamine 1.5 h after intraperitoneal administration of a single dose of 2 μmol/kg. The internalized conjugates were shown in red color. The nuclei of polycystic kidney, liver and spleen sections were stained with 1.0 μg/ml Hoechst 33342 (blue color). The tissue sections were imaged using Keyence BZ-9000 microscopy. Magnification, 20×; scale bar, 50 μm. High resolution images are shown in Supplementary Fig. 9. (For interpretation of the references to color in this figure legend, the reader is referred to the web version of this article.)

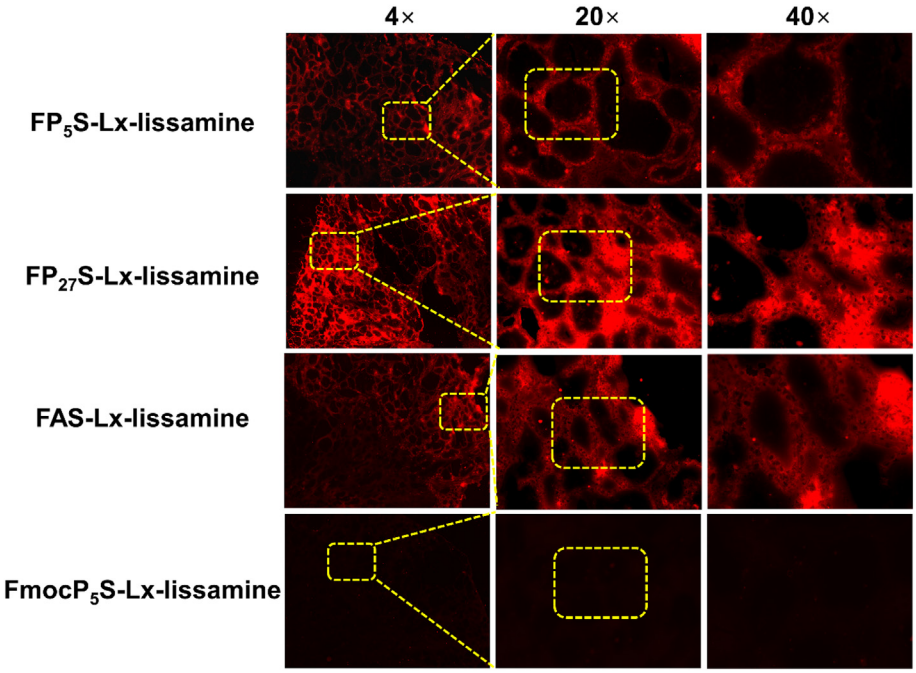

Fig. 11. Representative fluorescence images of polycystic kidney sections in 4×, 20× and 40× magnifications. High resolution images are shown in Supplementary Fig. 10.

3.6. Accumulation in polycystic kidney

To further compare the accumulation of FA-Lx-lissamine and $FmocP_5S$-Lx-lissamine conjugates in the polycystic kidneys, we constructed a composite image of 49 microscopic images taken at 20× magnification, thus providing a large overview of a transversal section of the kidney (Fig. 11). Magnifications at 20× and 40× further illustrate that all three folate targeted conjugates had accumulated efficiently in renal tissue, even despite the advanced stage of polycystic kidney disease which makes it difficult to identify unaffected tubular tissue. $FP_{27}S$-Lx-lissamine showed the strongest accumulation in the polycystic kidney in comparison to FP_5S-Lx-lissamine and FAS-Lx-lissamine, which may relate to relative hydrophilicity or differences in the extent and rates of distribution. The non-folate conjugate $FmocP_5S$-Lx-lissamine showed no accumulation in the kidney, thus demonstrating that kidney accumulation can be fully attributed to the FA-targeting moiety of the conjugates.

Our results are in good agreement with the study by Kipp et al., who used a folate-hapten conjugate to study uptake in the kidneys of PKD mice [15]. Using indirect immunofluorescence detection by anti-FITC immunostaining, kidney accumulation and uptake in cyst-lining epithelial cells was elegantly visualized in two different mouse models that represent ADPKD. Promising therapeutic results were achieved with a folate-rapamycin conjugate (FC-rapa), both in the bpk model [14] and the pkd−/− model [15] of PKD. Low dose treatment with FC-rapa (ranging from 0.1–0.6 nmol/kg/day; ~90–550 ng/kg/day) inhibited renal mTOR pathway activity (i.e. S6 phosphorylation), renal cyst index and renal fibrosis. FC-rapa was truly kidney-directed, as extrarenal mTOR activity (i.e. thymus mTOR) and systemic body weight were not affected [15]. Although we were not able to test therapeutic efficacy of FA-Lx-dactolisib conjugates at this moment, we expect similar promising activity as observed for FC-rapa, in view of the similar molecular target of rapamycin and dactolisib. Major differences between FC-rapa and FA-Lx-dactolisib conjugates are the employed linker chemistry and the dual inhibitory profile of dactolisib (PI3kinase and mTOR) versus rapamycin (mTOR). Regarding the linker chemistry, platinum(II)-linked conjugates show high stability in biological media and during circulation [71], in combination with sustained release during several days upon accumulation in target organs [55,68]. Such a sustained release profile will afford either once weekly administration or the targeted accumulation of drug levels by several loading doses that accumulate in cyst lining cells. Although promising results have been achieved with FC-rapa, in vivo stability in the circulation of this type of conjugate is expected to be poor, due to the presence of a disulfide and ester linkage (as shown for FC-everolimus which is similar in structure [13]).

3.7. Immunohistochemistry and histological analysis

Folate receptors are expressed on the apical brush-border membrane of kidney proximal tubular epithelial cells [72,73]. To determine whether folate receptors expression is maintained in polycystic kidneys in the iKsp-$Pkd1^{del}$ mice, kidney sections were stained with rabbit anti-folate primary antibody (PA5-24186, Thermofisher Scientific) and visualized with donkey anti-rabbit IgG (H+L) Alexa Fluor 488 secondary antibody. A transversal section of the kidney from the vehicle control group was stained to show the abundant expression of FR throughout the cross-section of the kidney in iKsp-$Pkd1^{del}$ mice, demonstrating that FR is highly expressed in this model of polycystic kidney disease (Fig. 12). In mice injected with the FA-Lx-lissamine conjugates, the red fluorescence signal representing the internalized conjugates was colocalized with green fluorescence signal, demonstrating that the folate targeted conjugates were internalized by cyst-lining epithelial cells via folate receptors. Of note, although uptake of FA-conjugates colocalized with FR, not all FA-positive areas stained positive for uptake of FA conjugates. Possible explanations for such untargeted areas in the polycystic kidney are the origin of the cystic tissue (originating from distal tubular cells rather than proximal tubular cells) or differences in perfusion or filtration which may have limited uptake of the conjugates. A more in-depth distribution study is warranted to address these questions.

4. Conclusions

We have developed kidney targeted FA-Lx-dactolisib and the corresponding FA-Lx-lissamine conjugates that exploit platinum linker

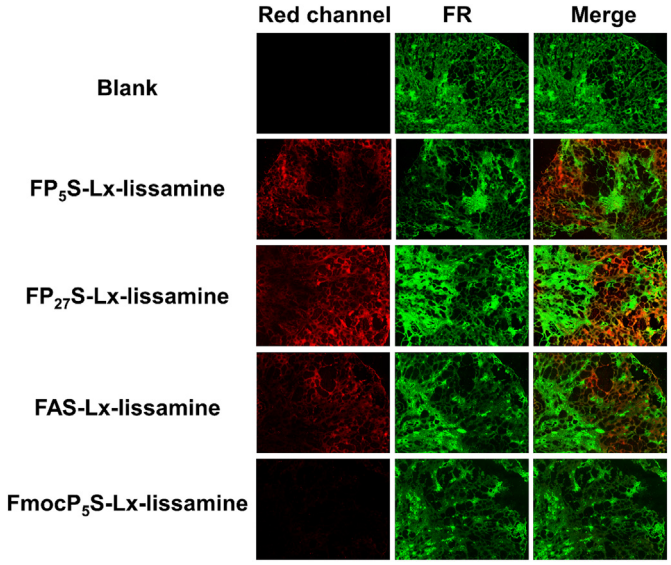

Fig. 12. Representative fluorescence images of polycystic kidney sections immunostaining with folate receptor on the proximal tubular cells of the polycystic kidneys 1.5 h after intraperitoneally administration of a single dose of 2 μmol/kg of PBS, three FA-Lx-lissamine conjugates and $FmocP_5S$-Lx-lissamine. The folate receptors were shown in green color and the internalized conjugates were shown in red color. High resolution images are shown in Supplementary Fig. 11. (For interpretation of the references to color in this figure legend, the reader is referred to the web version of this article.)

technology for coupling of the drug to the folate targeting ligand. The FA-Lx-dactolisib conjugates are stable in serum and culture medium while the drug is released in the presence of intracellular concentrations of glutathione. The FA-Lx-dactolisib conjugates display nanomolar inhibitory effect of mTOR and PI3K in FR-positive cultured kidney cells and are ineffective in FR-negative cells. A biodistribution study with FA-Lx-lissamine conjugates showed extensive accumulation in cyst-affected kidneys in accordance with FA-expression.

Acknowledgements

This work is supported by the China Scholarship Council (CSC) and the Dutch Technology Foundation STW (Project number 11823). All authors declared no conflict of interest.

Appendix A. Supplementary data

Supplementary data to this article can be found online at https://doi.org/10.1016/j.jconrel.2018.11.019.

References

[1] C.P. Leamon, J.A. Reddy, Folate-targeted chemotherapy, Adv. Drug Deliv. Rev. 56 (2004) 1127–1141.
[2] M.A. van Dongen, J.E. Silpe, C.A. Dougherty, A.K. Kanduluru, S.K. Choi, B.G. Orr, P.S. Low, M.M. Banaszak Holl, Avidity mechanism of dendrimer-folic acid conjugates, Mol. Pharm. 11 (2014) 1696–1706.
[3] J. Sudimack, R.J. Lee, Targeted drug delivery via the folate receptor, Adv. Drug Deliv. Rev. 41 (2000) 147–162.
[4] M. Srinivasarao, C.V. Galliford, P.S. Low, Principles in the design of ligand-targeted cancer therapeutics and imaging agents, Nat. Rev. Drug Discov. 14 (2015) 203–219.
[5] I.R. Vlahov, C.P. Leamon, Engineering folate-drug conjugates to target cancer: from chemistry to clinic, Bioconjug. Chem. 23 (2012) 1357–1369.
[6] Y. Lu, P.S. Low, Folate-mediated delivery of macromolecular anticancer therapeutic agents, Adv. Drug Deliv. Rev. 64 (2012) 342–352.
[7] R.M. Sandoval, M.D. Kennedy, P.S. Low, B.A. Molitoris, Uptake and trafficking of fluorescent conjugates of folic acid in intact kidney determined using intravital two-photon microscopy, Am. J. Phys. Cell Phys. 287 (2004) C517–C526.
[8] J. Selhub, I.H. Rosenberg, Demonstration of high-affinity folate binding activity associated with the brush border membranes of rat kidney, Proceedings of the National Academy of Sciences of the United States of America, Vol. 75 1978, pp. 3090–3093.
[9] T. Betzel, C. Muller, V. Groehn, A. Muller, J. Reber, C.R. Fischer, S.D. Kramer, R. Schibli, S.M. Ametamey, Radiosynthesis and preclinical evaluation of 3′-Aza-2′-[(18)F]fluorofolic acid: a novel PET radiotracer for folate receptor targeting, Bioconjug. Chem. 24 (2013) 205–214.
[10] C.J. Mathias, D. Hubers, P.S. Low, M.A. Green, Synthesis of [(99m)Tc]DTPA-folate and its evaluation as a folate-receptor-targeted radiopharmaceutical, Bioconjug. Chem. 11 (2000) 253–257.
[11] M.J. Turk, G.J. Breur, W.R. Widmer, C.M. Paulos, L.C. Xu, L.A. Grote, P.S. Low, Folate-targeted imaging of activated macrophages in rats with adjuvant-induced arthritis, Arthritis Rheum. 46 (2002) 1947–1955.
[12] Y. Lu, T.W. Stinnette, E. Westrick, P.J. Klein, M.A. Gehrke, V.A. Cross, I.R. Vlahov, P.S. Low, C.P. Leamon, Treatment of experimental adjuvant arthritis with a novel folate receptor-targeted folic acid-aminopterin conjugate, Arthritis Res. Ther. 13 (2011) R56.
[13] Y. Lu, N. Parker, P.J. Kleindl, V.A. Cross, K. Wollak, E. Westrick, T.W. Stinnette, M.A. Gehrke, K. Wang, H.K. Santhapuram, F. You, S.J. Hahn, J.F. Vaughn, P.J. Klein, I.R. Vlahov, P.S. Low, C.P. Leamon, Antiinflammatory activity of a novel folic acid targeted conjugate of the mTOR inhibitor everolimus, Mol. Med. 21 (2015) 584–596.
[14] J.M. Shillingford, C.P. Leamon, I.R. Vlahov, T. Weimbs, Folate-conjugated rapamycin slows progression of polycystic kidney disease, J. Am. Soc. Nephrol.: JASN 23 (2012) 1674–1681.
[15] K.R. Kipp, S.L. Kruger, M.F. Schimmel, N. Parker, J.M. Shillingford, C.P. Leamon, T. Weimbs, Comparison of folate-conjugated rapamycin versus unconjugated rapamycin in an orthologous mouse model of polycystic kidney disease, Am. J. Physiol.-Renal Physiol. 315 (2) (2018) F395–F405.
[16] H. Happe, D.J. Peters, Translational research in ADPKD: lessons from animal models, Nat. Rev. Nephrol. 10 (2014) 587–601.
[17] M.Y. Chang, A.C. Ong, Mechanism-based therapeutics for autosomal dominant polycystic kidney disease: recent progress and future prospects, Nephron. Clin. Pract. 120 (2012) c25–c34 (discussion c35).
[18] R.P. Wüthrich, C. Mei, Pharmacological management of polycystic kidney disease, Expert. Opin. Pharmacother. 15 (2014) 1085–1095.
[19] A. Hofherr, M. Kottgen, Polycystic kidney disease: Cilia and mechanosensation revisited, Nat. Rev. Nephrol. 12 (2016) 318–319.
[20] C.J. Willey, J.D. Blais, A.K. Hall, H.B. Krasa, A.J. Makin, F.S. Czerwiec, Prevalence of autosomal dominant polycystic kidney disease in the European Union, Nephrol. Dial. Transplant. 32 (2016) 1356–1363.
[21] V. Patel, R. Chowdhury, P. Igarashi, Advances in the pathogenesis and treatment of polycystic kidney disease, Curr. Opin. Nephrol. Hypertens. 18 (2009) 99–106.
[22] W.N. Leonhard, M. Zandbergen, K. Veraar, S. van den Berg, L. van der Weerd, M. Breuning, E. de Heer, D.J. Peters, Scattered deletion of PKD1 in kidneys causes a cystic snowball effect and recapitulates polycystic kidney disease, J. Am. Soc. Nephrol.: JASN 26 (2015) 1322–1333.
[23] J.M. Shillingford, N.S. Murcia, C.H. Larson, S.H. Low, R. Hedgepeth, N. Brown, C.A. Flask, A.C. Novick, D.A. Goldfarb, A. Kramer-Zucker, G. Walz, K.B. Piontek, G.G. Germino, T. Weimbs, The mTOR pathway is regulated by polycystin-1, and its inhibition reverses renal cystogenesis in polycystic kidney disease, Proc. Natl. Acad. Sci. U. S. A. 103 (2006) 5466–5471.
[24] V.E. Torres, P.C. Harris, Mechanisms of Disease: autosomal dominant and recessive polycystic kidney diseases, Nat. Clin. Pract. Nephrol. (2) (2006) 40–55 (quiz 55).
[25] W.N. Leonhard, A. van der Wal, Z. Novalic, S.J. Kunnen, R.T. Gansevoort, M.H. Breuning, E. de Heer, D.J.M. Peters, Curcumin inhibits cystogenesis by simultaneous interference of multiple signaling pathways: in vivo evidence from a Pkd1-deletion model, Am. J. Physiol. Ren. Physiol. 300 (2011) F1193–F1202.
[26] M. Boca, G. Distefano, F. Qian, A.K. Bhunia, G.G. Germino, A. Boletta, Polycystin-1 induces resistance to apoptosis through the phosphatidylinositol 3-kinase/Akt signaling pathway, J. Am. Soc. Nephrol.: JASN 17 (2006) 637–647.
[27] S.-M. Maira, F. Stauffer, J. Brueggen, P. Furet, C. Schnell, C. Fritsch, S. Brachmann, P. Chene, A. De Pover, K. Schoemaker, Identification and characterization of NVP-BEZ235, a new orally available dual phosphatidylinositol 3-kinase/mammalian target of rapamycin inhibitor with potent in vivo antitumor activity, Mol. Cancer Ther. 7 (2008) 1851–1863.
[28] T.J. Liu, D. Koul, T. Lafortune, N. Tiao, R.J. Shen, S.M. Maira, C. Garcia-Echevrria, W.K. Yung, NVP-BEZ235, a novel dual phosphatidylinositol 3-kinase/mammalian target of rapamycin inhibitor, elicits multifaceted antitumor activities in human gliomas, Mol. Cancer Ther. 8 (2009) 2204–2210.
[29] S. Schrauwen, J. Depreeuw, L. Coenegrachts, E. Hermans, D. Lambrechts, F. Amant, Dual blockade of PI3K/AKT/mTOR (NVP-BEZ235) and Ras/Raf/MEK (AZD6244) pathways synergistically inhibit growth of primary endometrioid endometrial carcinoma cultures, whereas NVP-BEZ235 reduces tumor growth in the corresponding xenograft models, Gynecol. Oncol. 138 (2015) 165–173.
[30] M.I. Carlo, A.M. Molina, Y. Lakhman, S. Patil, K. Woo, J. Deluca, C.-H. Lee, J.J. Hsieh, D.R. Feldman, R.J. Motzer, A phase Ib study of BEZ235, a dual inhibitor of phosphatidylinositol 3-kinase (PI3K) and mammalian target of rapamycin (mTOR), in patients with advanced renal cell carcinoma, Oncologist 21 (2016) 787–788d.
[31] T.H. Booij, H. Bange, W.N. Leonhard, K. Yan, M. Fokkelman, S.J. Kunnen, J.G. Dauwerse, Y. Qin, B. van de Water, G.J. van Westen, High-throughput phenotypic screening of kinase inhibitors to identify drug targets for polycystic kidney disease, SLAS Discov. 22 (2017) 974–984. Advancing Life Sciences R&D.
[32] Y. Liu, M. Pejchinovski, X. Wang, X. Fu, D. Castelletti, T.J. Watnick, A. Arcaro, J. Siwy, W. Mullen, H. Mischak, Dual mTOR/PI3K inhibition limits PI3K-dependent pathways activated upon mTOR inhibition in autosomal dominant polycystic kidney disease, Sci. Rep. 8 (2018) 5584.

[33] Y. Mochida, H. Cabral, Y. Miura, F. Albertini, S. Fukushima, K. Osada, N. Nishiyama, K. Kataoka, Bundled assembly of helical nanostructures in polymeric micelles loaded with platinum drugs enhancing therapeutic efficiency against pancreatic tumor, ACS Nano 8 (2014) 6724–6738.
[34] D.C. Waalboer, J.A. Muns, N.J. Sijbrandi, R.B. Schasfoort, R. Haselberg, G.W. Somsen, H.J. Houthoff, G.A. van Dongen, Platinum(II) as bifunctional linker in antibody-drug conjugate formation: coupling of a 4-nitrobenzo-2-oxa-1,3-diazole fluorophore to trastuzumab as a model, ChemMedChem 10 (2015) 797–803.
[35] J. Prakash, M.H. de Borst, M. Lacombe, F. Opdam, P.A. Klok, H. van Goor, D.K. Meijer, F. Moolenaar, K. Poelstra, R.J. Kok, Inhibition of renal rho kinase attenuates ischemia/reperfusion-induced injury, J. Am. Soc. Nephrol.: JASN 19 (2008) 2086–2097.
[36] M.M. Fretz, M.E. Dolman, M. Lacombe, J. Prakash, T.Q. Nguyen, R. Goldschmeding, J. Pato, G. Storm, W.E. Hennink, R.J. Kok, Intervention in growth factor activated signaling pathways by renally targeted kinase inhibitors, J. Control. Release 132 (2008) 200–207 official journal of the Controlled Release Society.
[37] N.J. Sijbrandi, E. Merkul, J.A. Muns, D.C. Waalboer, K. Adamzek, M. Bolijn, V. Montserrat, G.W. Somsen, R. Haselberg, P.J. Steverink, A novel platinum (II)–based bifunctional ADC linker benchmarked using 89Zr-Desferal and Auristatin F–conjugated Trastuzumab, Cancer Res. 77 (2017) 257–267.
[38] S. Gholizadeh, J.A. Kamps, W.E. Hennink, R.J. Kok, PLGA-PEG nanoparticles for targeted delivery of the mTOR/PI3kinase inhibitor dactolisib to inflamed endothelium, Int. J. Pharm. 548 (2) (2017) 747–758.
[39] G. Nkepang, M. Bio, P. Rajaputra, S.G. Awuah, Y. You, Folate receptor-mediated enhanced and specific delivery of far-red light-activatable prodrugs of combretastatin A-4 to FR-positive tumor, Bioconjug. Chem. 25 (2014) 2175–2188.
[40] M. Ahir, S. Bhattacharya, S. Karmakar, A. Mukhopadhyay, S. Mukherjee, S. Ghosh, S. Chattopadhyay, P. Patra, A. Adhikary, Tailored-CuO-nanowire decorated with folic acid mediated coupling of the mitochondrial-ROS generation and miR425-PTEN axis in furnishing potent anti-cancer activity in human triple negative breast carcinoma cells, Biomaterials 76 (2016) 115–132.
[41] F. Lin, G. Chandrasekaran, M.C. de Gooijer, J.H. Beijnen, O. van Tellingen, Determination of NVP-BEZ235, a dual PI3K and mTOR inhibitor, in human and mouse plasma and in mouse tissue homogenates by reversed-phase high-performance liquid chromatography with fluorescence detection, J. Chromatogr. B Anal. Technol. Biomed. Life Sci. 901 (2012) 9–17.
[42] L. Graña-Suárez, W. Verboom, J. Huskens, Fluorescent supramolecular nanoparticles signal the loading of electrostatically charged cargo, Chem. Commun. 52 (2016) 2597–2600.
[43] E. Vlashi, L.E. Kelderhouse, J.E. Sturgis, P.S. Low, Effect of folate-targeted nanoparticle size on their rates of penetration into solid tumors, ACS Nano 7 (2013) 8573–8582.
[44] I.R. Vlahov, H.K. Santhapuram, F. You, Y. Wang, P.J. Kleindl, S.J. Hahn, J.F. Vaughn, D.S. Reno, C.P. Leamon, Carbohydrate-based synthetic approach to control toxicity profiles of folate-drug conjugates, J. Organ. Chem. 75 (2010) 3685–3691.
[45] K. Temming, M. Lacombe, P. van der Hoeven, J. Prakash, T. Gonzalo, E.C. Dijkers, L. Orfi, G. Kéri, K. Poelstra, G. Molema, Delivery of the p38 MAPkinase inhibitor SB202190 to angiogenic endothelial cells: development of novel RGD-equipped and PEGylated drug − albumin conjugates using platinum (II)-based drug linker technology, Bioconjug. Chem. 17 (2006) 1246–1255.
[46] T. Gonzalo, L. Beljaars, M. van de Bovenkamp, K. Temming, A.M. van Loenen, C. Reker-Smit, D.K. Meijer, M. Lacombe, F. Opdam, G. Keri, L. Orfi, K. Poelstra, R.J. Kok, Local inhibition of liver fibrosis by specific delivery of a platelet-derived growth factor kinase inhibitor to hepatic stellate cells, J. Pharmacol. Exp. Ther. 321 (2007) 856–865.
[47] M. Wang, Y. Miura, K. Tsuchihashi, K. Miyano, O. Nagano, M. Yoshikawa, A. Tanabe, J. Makino, Y. Mochida, N. Nishiyama, H. Saya, H. Cabral, K. Kataoka, Eradication of CD44-variant positive population in head and neck tumors through controlled intracellular navigation of cisplatin-loaded nanomedicines, J. Control. Release 230 (2016) 26–33 official journal of the Controlled Release Society.
[48] M. Beija, C.A. Afonso, J.M. Martinho, Synthesis and applications of Rhodamine derivatives as fluorescent probes, Chem. Soc. Rev. 38 (2009) 2410–2433.
[49] T. Gonzalo, E.G. Talman, A. van de Ven, K. Temming, R. Greupink, L. Beljaars, C. Reker-Smit, D.K. Meijer, G. Molema, K. Poelstra, R.J. Kok, Selective targeting of pentoxifylline to hepatic stellate cells using a novel platinum-based linker technology, J. Control. Release (111) (2006) 193–203 official journal of the Controlled Release Society.
[50] V. Serra, B. Markman, M. Scaltriti, P.J. Eichhorn, V. Valero, M. Guzman, M.L. Botero, E. Llonch, F. Atzori, S. Di Cosimo, M. Maira, C. Garcia-Echeverria, J.L. Parra, J. Arribas, J. Baselga, NVP-BEZ235, a dual PI3K/mTOR inhibitor, prevents PI3K signaling and inhibits the growth of cancer cells with activating PI3K mutations, Cancer Res. 68 (2008) 8022–8030.
[51] T.-J. Liu, D. Koul, T. Lafortune, N. Tiao, R.J. Shen, S.-M. Maira, C. Garcia-Echevrria, W.K.A. Yung, NVP-BEZ235, a novel dual phosphatidylinositol 3-kinase/mammalian target of rapamycin inhibitor, elicits multifaceted antitumor activities in human gliomas, Am. Assoc. Cancer Res. 8 (2009) 2204–2210.
[52] H. Wu, H. Shi, Y. Wang, X. Jia, C. Tang, J. Zhang, S. Yang, Hyaluronic acid conjugated graphene oxide for targeted drug delivery, Carbon 69 (2014) 379–389.
[53] M.H. Ta, D.C. Harris, G.K. Rangan, Role of interstitial inflammation in the pathogenesis of polycystic kidney disease, Nephrology 18 (2013) 317–330.
[54] J.A. Reddy, R. Dorton, E. Westrick, A. Dawson, T. Smith, L.C. Xu, M. Vetzel, P. Kleindl, I.R. Vlahov, C.P. Leamon, Preclinical evaluation of EC145, a folate-vinca alkaloid conjugate, Cancer Res. 67 (2007) 4434–4442.
[55] M. Dolman, K. Van Dorenmalen, E. Pieters, M. Lacombe, J. Pato, G. Storm, W. Hennink, R. Kok, Imatinib-ULS-lysozyme: a proximal tubular cell-targeted conjugate of imatinib for the treatment of renal diseases, J. Control. Release 157 (2012) 461–468.
[56] H. Uchino, Y. Matsumura, T. Negishi, F. Koizumi, T. Hayashi, T. Honda, N. Nishiyama, K. Kataoka, S. Naito, T. Kakizoe, Cisplatin-incorporating polymeric micelles (NC-6004) can reduce nephrotoxicity and neurotoxicity of cisplatin in rats, Br. J. Cancer 93 (2005) 678–687.
[57] C. Zhang, C. Li, Y. Liu, J. Zhang, C. Bao, S. Liang, Q. Wang, Y. Yang, H. Fu, K. Wang, D. Cui, Gold nanoclusters-based nanoprobes for simultaneous fluorescence imaging and targeted photodynamic therapy with superior penetration and retention behavior in tumors, Adv. Funct. Mater. 25 (2015) 1314–1325.
[58] L. Novo, E. Mastrobattista, C.F. van Nostrum, W.E. Hennink, Targeted decationized polyplexes for cell specific gene delivery, Bioconjug. Chem. 25 (2014) 802–812.
[59] Y. Bae, N. Nishiyama, K. Kataoka, In vivo antitumor activity of the folate-conjugated pH-sensitive polymeric micelle selectively releasing Adriamycin in the intracellular acidic compartments, Bioconjug. Chem. 18 (2007) 1131–1139.
[60] R.J. Lee, P.S. Low, Delivery of liposomes into cultured KB cells via folate receptor-mediated endocytosis, J. Biol. Chem. 269 (1994) 3198–3204.
[61] S. Wang, R.J. Lee, C.J. Mathias, M.A. Green, P.S. Low, Synthesis, purification, and tumor cell uptake of 67Ga-deferoxamine–folate, a potential radiopharmaceutical for tumor imaging, Bioconjug. Chem. 7 (1996) 56–62.
[62] C.P. Leamon, I.R. Vlahov, J.A. Reddy, M. Vetzel, H.K. Santhapuram, F. You, A. Bloomfield, R. Dorton, M. Nelson, P. Kleindl, J.F. Vaughn, E. Westrick, Folate-vinca alkaloid conjugates for cancer therapy: a structure-activity relationship, Bioconjug. Chem. 25 (2014) 560–568.
[63] U. Lachelt, V. Wittmann, K. Muller, D. Edinger, P. Kos, M. Hohn, E. Wagner, Synthetic polyglutamylation of dual-functional MTX ligands for enhanced combined cytotoxicity of poly(I:C) nanoplexes, Mol. Pharm. 11 (2014) 2631–2639.
[64] W.A. Henne, S.A. Kularatne, J. Hakenjos, J.D. Carron, K.L. Henne, Synthesis and activity of a folate targeted monodisperse PEG camptothecin conjugate, Bioorg. Med. Chem. Lett. 23 (2013) 5810–5813.
[65] E. Vlashi, J.E. Sturgis, M. Thomas, P.S. Low, Real time, noninvasive imaging and quantitation of the accumulation of ligand-targeted drugs into receptor-expressing solid tumors, Mol. Pharm. 6 (2009) 1868–1875.
[66] F. Ditrói, F. Tárkányi, S. Takács, A. Hermanne, Extension of activation cross section data of long lived products in deuteron induced nuclear reactions on platinum up to 50 MeV, Nucl. Instrum. Methods Phys. Res., Sect. B 401 (2017) 56–70.
[67] R. del Campo, J.J. Criado, E. García, M.R. Hermosa, A. Jimenez-Sanchez, J.L. Manzano, E. Monte, E. Rodrıguez-Fernández, F. Sanz, Thiourea derivatives and their nickel (II) and platinum (II) complexes: antifungal activity, J. Inorg. Biochem., 89 (2002) 74–82.
[68] J. Prakash, M. Sandovici, V. Saluja, M. Lacombe, R.Q. Schaapveld, M.H. de Borst, H. van Goor, R.H. Henning, J.H. Proost, F. Moolenaar, G. Keri, D.K. Meijer, K. Poelstra, R.J. Kok, Intracellular delivery of the p38 mitogen-activated protein kinase inhibitor SB202190 [4-(4-fluorophenyl)-2-(4-hydroxyphenyl)-5-(4-pyridyl) 1H-imidazole] in renal tubular cells: a novel strategy to treat renal fibrosis, J. Pharmacol. Exp. Ther. 319 (2006) 8–19.
[69] K. Temming, M. Lacombe, P. van der Hoeven, J. Prakash, T. Gonzalo, E.C. Dijkers, L. Orfi, G. Kéri, K. Poelstra, G. Molema, Delivery of the p38 MAPkinase inhibitor SB202190 to angiogenic endothelial cells: development of novel RGD-equipped and PEGylated drug-albumin conjugates using platinum (II)-based drug linker technology, Bioconjug. Chem. 17 (2006) 1246–1255.
[70] N.Q. Vinh, S. Naka, H. Cabral, H. Murayama, S. Kaida, K. Kataoka, S. Morikawa, T. Tani, MRI-detectable polymeric micelles incorporating platinum anticancer drugs enhance survival in an advanced hepatocellular carcinoma model, Int. J. Nanomedicine 10 (2015) 4137–4147.
[71] J.A. Muns, V. Montserrat, H.-J. Houthoff, K. Codée-Van Der Schilden, O. Zwaagstra, N.J. Sijbrandi, E. Merkul, G.A. van Dongen, In vivo characterization of platinum (II)-based linker technology for the development of antibody–drug conjugates: taking advantage of dual labeling with 195mPt and 89Zr, J. Nucl. Med. 59 (2018) 1146–1151.
[72] Y. Bae, S. Fukushima, A. Harada, K. Kataoka, Design of environment-sensitive supramolecular assemblies for intracellular drug delivery: polymeric micelles that are responsive to intracellular pH change, Angew. Chem. Int. Ed. 42 (2003) 4640–4643.
[73] H. Birn, O. Spiegelstein, E.I. Christensen, R.H. Finnell, Renal tubular reabsorption of folate mediated by folate binding protein 1, J. Am. Soc. Nephrol. 16 (2005) 608–615.